Editor's comment:

Thank you again for your patience. The original reviewers requested to see the revised manuscript, and thus, I allowed them to re-review it. I've finally heard back from both reviewers. They agree the manuscript is much improved and should be accepted; however, one reviewer requested you address the very minor comments I've copied below. Once you address these final comments, I'll immediately accept as is.

Thanks again, Jason Surratt

Remaining comments from one of the reviewers:

"The authors clearly took the reviewers comments into account and I think that the manuscript has been improved significantly, for example the addition of the science questions in the Introduction section was very helpful. I just have a few small additional comments.

1.) The addition of Table 1 was important, but I still would like to see a little more details on the instruments such as the sensitivity and limits of detection.

2.) The diurnal variations of the trace gases that are in the supplement should be in the main text combined with the meteorological parameters in Figure 5.

3.) In Figure 3, I meant to have CO on a linear AND a log scale.

4.) How confident are you in the ozone data in Figure 5? If there are cross contaminations in the ozone data should they be included in this Figure or taken out here as well. If the data are used the interference has to be discussed in detail and described, which data are still useful.

5.) The outcomes of SAFIRED section is now much improved and very useful.

Author's response:

The author's thank the editor and reviewers for the suggestions and comments. Table 1 has been expanded to include more instrumental details such as detection limits and uncertainties where available. The diurnal trends of trace gases from the supplementary material has been combined in the main body within Figure 5. The CO time series in FIgure 3 now shows both a linear and a log scale. Periods of data when interferences were suspected in ozone measurements have been excluded from Figure 6. This has been briefly explained in the experimental section. This was done by investigating periods of strong biomass burning signals (using e.g. acetonitrile as a marker) and removing periods where concentrations were high and well correlated with ozone (they should not be co-emitted).

Formatted: Font:Bold, Underline

Formatted: Font:Bold, Underline

Title: Biomass burning emissions in north Australia during the early dry season: an overview of the 2014 SAFIRED campaign

Authors:

Marc D. Mallet[1], Maximilien J. Desservettaz[2], Branka Miljevic[1*], Andelija Milic[1], Zoran D. Ristovski[1], Joel Alroe[1], Luke T. Cravigan[1], E. Rohan Jayaratne[1], Clare Paton-Walsh[2], David W.T. Griffith[2], Stephen R. Wilson[2], Graham Kettlewell[2], Marcel V. van der Schoot[3], Paul Selleck[3], Fabienne Reisen[3], Sarah J. Lawson[3], Jason Ward[3], James Harnwell[3], Min Cheng[3], Rob W. Gillett[3], Suzie B. Molloy[3], Dean Howard[4], Peter F. Nelson[4], Anthony L. Morrison[4], Grant C. Edwards[4], Alastair G. Williams[5], Scott D. Chambers[5], Sylvester Werczynski[5], Leah R. Williams[6], V. Holly L. Winton[7,n], Brad Atkinson[8], Xianyu Wang[9], Melita D. Keywood[3*]

Affiliations:

[1]Department of Chemistry, Physics and Mechanical Engineering, Queensland University of Technology, Queensland, Brisbane, 4000, Australia

[2]Centre for Atmospheric Chemistry, University of Wollongong, Wollongong, New South Wales, 2522, Australia

[3]CSIRO Oceans and Atmosphere, Aspendale, Victoria, 3195, Australia

[4]Department of Environmental Sciences, Macquarie University, Sydney, New South Wales, 2109, Australia

[5]Australian Nuclei Science and Technology Organisation, Sydney, New South Wales, 2232, Australia

[6]Aerodyne Research, Inc., Billerica, Massachusetts, 01821, USA

[7]Physics and Astronomy, Curtin University, Perth, Western Australia, 6102, Australia

[8]Bureau of Meteorology, Darwin, Northern Territory, 0810, Australia

[9]National Research Centre for Environmental Toxicology, Brisbane, Queensland, 4108, Australia

[n]Now at the British Antarctic Survey, Cambridge, CB3 0ET, United Kingdom

Formatted: Font color: Text 1

Comment [MM1]: R2:

This paper gives an overview of the SAFIRED2014 campaign in Northern Australia aimed at investigating biomass burning in an area that has very frequent burning but is clearly understudied. This paper suffers from the typical issues of overview papers, where there is a long introduction of instruments and methods, but no actual results. In this paper especially the last section "Outcomes of SAFIRED" is very long, includes short literature reviews, but teases at potential results and points to other related papers without giving any results. Overview papers clearly serve a purpose and should include four major points: 1) description of the science goals and how the campaign was designed to answer them, 2) a systematic description of the used instrumenta- tion, 3) a big picture overview of the results and 4) a conclusion of how the campaign results are usable for answering the science question. This overview paper here de- scribes most of the above points, but could benefit from some improvements and in particular would benefit from summarizing the results more systematically.

Comment [MM2]: R3:

Mallet et al. provide an overview of the multi-institutional measurement campaign con- ducted in Northern Australia during the dry season to measure the emissions and transformations of trace gases and particles emitted by savannah and grassland fires. The motivation for the measurement campaign is novel, the manuscript is well written and the results are appropriately described. The measurements from this campaign are likely to improve our understanding of biomass burning emissions at the local and global scale. The only major concern I have is that the manuscript, being an overview article, could be improved in terms of the presentation of the campaign specific information and data (see comment #s 3, 4, 5, 11, 12). This would make the manuscript much more citable and a serve as a gateway for anyone interested in SAFIRED-related literature. I recommend publication of the manuscript after the following minor comments have been addressed and/or clarified.

Formatted: Font color: Text 1

Formatted: Normal

Deleted: National Environmental Research Council,

Deleted: 0HT

Formatted: Font color: Text 1

Deleted: K

Formatted: Font color: Text 1

***Corresponding Authors:**

Dr Melita Keywood

Contact Phone: +613 9239 4596

Contact Email: melita.keywood@csiro.au

Dr Branka Miljevic

Contact Phone: +61 7 3138 3827

Contact Email: b.miljevic@qut.edu.au

Keywords:

Biomass burning | savannah fires | greenhouse gases | aerosols | mercury

Abstract

The SAFIRED (Savannah Fires in the Early Dry Season) campaign took place from 29th of May, 2014 until the 30th June, 2014 at the Australian Tropical Atmospheric Research Station (ATARS) in the Northern Territory, Australia. The purpose of this campaign was to investigate emissions from fires in the early dry season in northern Australia. Measurements were made of biomass burning aerosols, volatile organic compounds, polycyclic aromatic carbons, greenhouse gases, radon, speciated atmospheric mercury, and trace metals. Aspects of the biomass burning aerosol emissions investigated included; emission factors of various species, physical and chemical aerosol properties, aerosol aging, micronutrient supply to the ocean, nucleation, and aerosol water uptake. Over the course of the month-long campaign, biomass burning signals were prevalent and emissions from several large single burning events were observed at ATARS.

Biomass burning emissions dominated the gas and aerosol concentrations in this region. Dry season fires are extremely frequent and widespread across the northern region of Australia, which suggests that the measured aerosol and gaseous emissions at ATARS are likely representative of signals across the entire region of north Australia. Air mass forward trajectories show that these biomass burning emissions are carried north west over the Timor Sea and could influence the atmosphere over Indonesia and the tropical atmosphere over the Indian Ocean. Here we present characteristics of the biomass burning observed at the sampling site and provide an overview of the more specific outcomes of the SAFIRED campaign.

Comment [MM3]: R1:

Abstract; This section is too long and needs to be tightened up considerably.

Deleted: mercury cycle

Comment [MM4]: R1:
Line 45. How does one measure the "mercury cycle"? It is possible to measure the chemical species that make up the mercury cycle.

Formatted: Font color: Text 1

Deleted: emitted

Formatted: Font color: Text 1

Formatted: Justified, Indent: First line: 0.39", Line spacing: double

Deleted: . Nine major biomass burning events were identified and associated with intense or close individual smoke plumes

Formatted: Font color: Text 1

Deleted: .

Formatted: Font color: Text 1

Formatted: Font color: Text 1

Formatted: Font color: Text 1

1. Introduction

Tropical north Australia is dominated by savannah ecosystems. This region consists of dense native and exotic grasslands and scattered trees and shrubs. Conditions are hot, humid and wet in the summer months of December through March with hot, dry conditions for the rest of the year giving rise to frequent fires between June and November each year. Human settlements are relatively scarce in northern Australia, outside of the territory capital, Darwin (population of 146 000). To the north of the continent are the tropical waters of the Timor Sea, as well as the highly populated Indonesian archipelago. South of the savannah grasslands are the Tanami, Simpson and Great Sandy Deserts, spanning hundreds of thousands of square kilometers. Emissions from fires in the savannah regions of northern Australia are therefore the most significant regional source of greenhouse and other trace gases, as well as atmospheric aerosol. Globally, savannah and grassland fires are the largest source of carbon emissions from biomass burning(van der Werf et al., 2010;Shi et al., 2015) and play a significant role in the earth's radiative budget. It is therefore important to quantify, characterise and fully understand the emissions from savannah fires in northern Australia, taking into account the complexity, variability and diversity of the species emitted.

In Australia approximately 550 000 km^2 of tropical and arid savannahs burn each year (Meyer et al., 2012;Russell-Smith et al., 2007), representing 7% of the continent's land area. In the tropical north of Australia, the fires during the early dry season in May/June consist of naturally occurring and accidental fires, as well as prescribed burns under strategic fire management practice to reduce the frequency and intensity of more extensive fires in the late dry season in October and November (Andersen et al., 2005).

Comment [MM8]: R3:
While some of the relevant literature has been cited, it would be worthwhile to discuss (likely in the Introduction) similar measurement campaigns performed in other parts of the world that have examined emissions from biomass burning and how those earlier lab and field efforts (e.g., BBOP, SCREAM, FLAME1-5, etc) have helped inform critical gaps, research questions, instrumentation, analysis techniques etc. for the SAFIRED campaign.

Comment [MM9]: R3:
Being an overview article, I think the manuscript could benefit from a schematic and/or cartoon in the introduction that sketches the region of interest (Northern Aus- tralia) and caricatures the emissions, processes and impacts being studied in detail in this campaign. Furthermore, a bulleted list in the beginning of the manuscript that lists the research/science questions for SAFIRED would provide context for the various measurements and analysis performed.

Formatted: Font color: Text 1

Comment [MM10]: R1:

Lines 80 and 81. Savannah and grassland fires are not the largest source of carbon to the atmosphere, as is clear when comparing the numbers from the quoted references with the global anthropogenic source of CO_2 for example. Do the authors mean the largest source of black carbon?

Formatted: Font color: Text 1

Formatted: Font color: Text 1

Formatted: Font color: Text 1

Formatted: Font color: Text 1

Formatted: Font color: Text 1

Formatted: Font color: Text 1

These fires in the early dry season burn with a low to moderate intensity and are normally confined to the grass-layer. Events where fires reach the canopy level are rare. These prescribed burns are an important process for the region and are undertaken by local landholders with permits, as well as government supported bodies and volunteers. There has been a recent push to reinstate traditional Aboriginal fire management regimes in this region (Russell-Smith et al., 2013). Other fire management regimes are implemented in similar environments around the world, such as the savannah ecosystems of Africa (Govender et al., 2006) or the chaparral grasses in the United States (Akagi et al., 2012). In general, fire management regimes are considered to benefit regional biodiversity and can lead to the long-term increase in living biomass, resulting in a reduction of greenhouse gas emissions (Russell-Smith et al., 2013). Quantifying the emissions from dry season fires on regional scales is essential for understanding the impact of these fires on the local and global atmosphere.

The components and concentrations of emissions from savannah fires are dependent upon the vegetation and burning conditions. While CO_2 is the primary product of biomass burning (BB), combustion processes also result in the emission of many other trace gases such as CO, CH_4, NOx, N_2O as well as non methane organic compounds (NMOCs) and aerosol particles composed of elemental carbon, organic carbon and some inorganic material (Crutzen and Andreae, 1990). The state of organics in biomass burning aerosols can vary significantly due to the type of plant material burned, the characteristics of the fires themselves as well as through aging processes in the atmosphere.

Formatted: Font color: Text 1
Formatted: Font color: Text 1
Formatted: Font color: Text 1
Formatted: Font color: Text 1
Formatted: Font color: Text 1
Formatted: Font color: Text 1
Formatted: Font color: Text 1
Formatted: Font color: Text 1
Deleted: incomplete
Formatted: Font color: Text 1
Deleted: s
Comment [MM11]: R1:

Line 109. NOx is not an incomplete combustion product, in fact NO is most definitely a flaming stage compound. The authors would know this if they referred to the numerous references that have come after Crutzen and Andreae [1990], Akagi et al [2011] (referenced later on)s is a nice recent review of BB emissions.
Formatted: Font color: Text 1
Formatted: Font color: Text 1
Formatted: Font color: Text 1

The effects of these emissions on radiative forcing are complex. The global average radiative forcing due to biomass burning aerosol-radiation interaction is estimated in the 5th International Panel on Climate Change report as 0.0 W m^{-2} with an uncertainty range of -0.20 to +0.20 Wm^{-2} (Bindoff et al., 2013). It is well known that greenhouse gases have a positive radiative forcing, heating up the atmosphere. Light absorbing carbon in the aerosol phase will also result in a positive radiative forcing (Jacobson, 2001) by absorbing shortwave radiation. Conversely, the presence of aerosol organic and inorganic matter can result in a negative radiative forcing by scattering solar radiation (Penner et al., 1998). In addition, biomass burning has been shown to be a significant source of cloud condensation nuclei (CCN), despite typically being composed of weakly hygroscopic substances (Lawson et al., 2015), due to the high number of particles emitted. This can result in a change in cloud droplet concentrations and volume, thereby influencing cloud formation, albedo and lifetime. The contribution of each species to the overall radiative forcing is also likely to change as smoke plumes age (Liousse et al., 1995). Furthermore, not all biomass burning aerosol will interact with radiation in the same way. For example, fresh BB emissions in the tropics has been observed to be more absorbing than those from boreal forest fires(Wong and Li, 2002). The role of biomass burning emissions is not limited to the Earth's radiative budget. Certain species of emissions (e.g., mercury) can be deposited and sequestered in soil (Gustin et al., 2008), vegetation (Rea et al., 2002) or bodies of water (LaRoche and Breitbarth, 2005).

Large-scale studies in Africa (Keil and Haywood, 2003), North America (Yokelson et al., 2009;Singh et al., 2006), Europe (Saarikoski et al., 2007), South America (Ferek et al., 1998) and Asia (Lin et al., 2013;Du et al., 2011) have provided valuable insight into

Formatted: Normal

the impact of fire emissions on the regional atmosphere and laboratory measurements have proved to be useful in understanding the emission factors, composition and atmospheric processing of these emissions (Stockwell et al., 2014). Despite this, there is still a need for a better scientific understanding of the influence biomass burning has on atmospheric composition and air quality (Kaiser and Keywood, 2015), particularly around Australia. Furthermore, the tropics are disproportionately under-sampled and the atmospheric and ocean processes in these regions are of both regional and global consequence. The SAFIRED campaign will contribute towards better understanding biomass burning emissions and the atmospheric composition in tropical Australia.

On a more specific level, the SAFIRED campaign was undertaken with the following objectives:

- To obtain Australian savannah fire dry season emission factors for greenhouse gases, polycyclicaromatic hydrocarbons, gaseous elemental mercury, non-methane organic compounds, Aitken and accumulation mode aerosols and non-refractory submicron organic, sulfates, ammonia, nitrates and chlorides.
- To understand the emission of mercury from north Australian fires and to quantify the delivery of mercury to the ecosystem.
- To characterise the composition and size of aerosols in the region of north Australia and to understand the influence and extent of biomass burning on the total aerosol burden.
- To assess the ability of biomass burning aerosol to act as cloud condensation nuclei and to establish a link between aerosol composition, size and CCN.

Deleted: There

Formatted: Font color: Text 1

Formatted: Font color: Text 1

Deleted: .

Formatted: Font color: Text 1

Comment [MM12]: R2:

I think it would be helpful to actually list the specific science questions at the end of the introduction or in a new section before the instrument descriptions.

Formatted: List Paragraph, Bulleted + Level: 1 + Aligned at: 0.25" + Indent at: 0.5"

Formatted: Font color: Text 1

- To assess the fractional solubility of aerosol iron and other trace metals in this region in the context of the potential supply of micronutrients required for marine primary production in the ocean.

Formatted: Font color: Text 1

2. Description of experiment

2.1 Site

Formatted: Heading 2

The Australian Tropical Atmospheric Research Station (ATARS; 12°14'56.6"S, 131°02'40.8"E) is located on the Gunn Point peninsula in northern Australia (see Figure 1). ATARS is operated by the Australian Bureau of Meteorology and the CSIRO (Commonwealth Scientific and Industrial Research Organisation). Standard meteorological measurements (wind velocity, atmospheric pressure, precipitation) run permanently at ATARS and two laboratories are in place for the installation of other instruments. The SAFIRED campaign took place from 29th May 2014 until the 30th June 2014, with personnel and instruments from nine institutes utilising these laboratories to make comprehensive gaseous and aerosol measurements during this period of the early dry season.

2.2 Instruments and measurements

Comment [MM13]: R2:
The chapter 2.2 Instruments and Measurements should be made more consistent be- tween the individual instrument descriptions and also misses some critical information. Most of the instrument detection methods are described well, but the most important information for all the measurements are missing. For each instrument description the following needs to be added: sensitivity (precision and accuracy), limit of detection, time resolution and used inlet. A table should be added that lists all of these instrument parameters and also a reference to the technique.

Comment [MM14]: R3:
In the methods section, the manuscript could benefit from a Table that lists the in- strument, quantity measured, accuracy/precision, frequency. For example, see Figure 1b, 1c, 2b, 2c, etc in Ryerson et al., (JGR, 2013).

Formatted: Heading 2

Deleted:

Table 1 A summary of the quantities measured during SAFIRED and the respective instrument or measurement technique. Detection limits and uncertainties are expressed for select instruments or measurements.

Quantity	Instrument or Technique	Sample frequency	Reference	Detection limits	Uncertainties
CO, CO_2, CH_4 and N_2O	Fourier transform infrared spectrometry	3 minute	(Griffith et al., 2012)	0.04 mg CO_2 $m^{-2}s^{-1}$, 20 ngN $m^{-2}s^{-1}$ (N_2O), 30 ng CH_4 $m^{-2}s^{-1}$)	0.02 (CO_2), 0.2 (CH_4), 0.1 (N_2O), 0.2 (CO) [a]
O_3	UV Photometric Ozone Analysis	1 minute		0.50 ppb	~1 ppb
Non methane organic compounds	Proton Transfer-Mass Spectrometry, high performance liquid chromatography of Supelco cartridge samples; gas chromatography of adsorbant tubes	3 minute; 12 hour; 12 hour	(Galbally et al., 2007); (Cheng et al., 2016); (Lawson et al., 2015, Dunne et al. (2017))	2 - 563 ppt (PTR-MS ions)	<22% (PTR-MS ions)
Polycyclic aromatic hydrocarbons (gas and particle phase)	Gas chromatography and high resolution mass spectrometry of filter and foam samples	24 hour	(Wang et al., 2017)	<1 pg m^{-3}	<±20% (rep)
Gaseous elemental mercury; gaseous oxidised mercury; and particulate-bound mercury	Cold vapour atomic fluorescence spectroscopy	5 minute; 2 hour; 2 hour	(Landis et al., 2002); (Steffen et al., 2008)	0.1 ng m^{-3} (GEM), 2 pg m^{-3} (GOM), 2 pg m^{-3} (PBM)	N.R. [b]
Radon	700L dual-flow two filter detector	1 hour	(Chambers et al., 2014)	±0.04 Bq m^{-3}	10 - 14%
Aerosol mobility size distributions (14 nm to 670 nm); neutral and charged aerosol size distributions (0.8 nm to 42 nm)	Scanning mobility particle sizer, Neutral cluster and air ion spectrometry	5 minute; 4 minute	(Mirme et al., 2007)	-	±1% in size selection, ±10% in CPC counts
Cloud condensation nuclei concentration (at 0.5% supersaturation)	Supersaturated streamwise continuous-flow of aerosols in a wetted column using thermal-gradient followed by Optical Particle Counting of activated CCN	10 second	(Gras et al., 2007)	-	±0.1% SS, ±20% in OPC counts
Elemental and organic carbon; water soluble ions; and anhydrous sugars (PM_1 and PM_{10})	β+ attenuation; ion chromatography; high performance anion-exchange chromatography	12 hour	(Chow et al., 2007b); (Iinuma et al., 2009)	0.0009 µg m^{-3} (oxalate), 0.0002 µg m^{-3} (levoglucosan)	N.R.
Soluble and total fraction of trace metals (PM_{10})	High-resolution inductively coupled plasma mass spectrometry analysis of extracted leachates and digests.	24 hour	(Winton et al., 2016)	< 1 pg m^{-3}	±5% in soluble Fe, ±3% in total Fe
Non-refractory chemical composition (PM_1)	Time-of-flight aerosol mass spectrometry	3 minute	(Drewnick et al., 2005)	0.003 µg m^{-3} (NO_3^-, SO_4^{2-}), 0.03 µg m^{-3} (NH_4^+, organics)	~±20%
Aerosol volatility and hygroscopicity (50 nm and 150 nm)	Volatility and hygroscopicity tandem differential mobility analysis	12 minute (full cycle)	(Johnson et al., 2004)	-	±1% in size sselection, ±1% in RH, ±3% in thermodenuder temperature

Formatted ... [1]
Formatted ... [2]
Formatted Table ... [3]
Formatted ... [4]
Formatted ... [5]
Formatted ... [6]
Formatted ... [7]
Formatted ... [8]
Formatted ... [9]
Formatted ... [10]
Formatted ... [11]
Formatted ... [12]
Formatted ... [13]
Formatted ... [14]
Formatted ... [16]
Formatted ... [15]
Formatted ... [17]
Formatted ... [18]
Formatted ... [19]
Formatted ... [20]
Formatted ... [22]
Formatted ... [23]
Formatted ... [24]
Formatted ... [21]
Formatted ... [26]
Formatted ... [27]
Formatted ... [28]
Formatted ... [25]
Formatted ... [30]
Formatted ... [32]
Formatted ... [31]
Formatted ... [29]
Formatted ... [33]
Formatted ... [34]
Formatted ... [36]
Formatted ... [35]

[a] Uncertainty expressed as measurement precision (Allan deviation) for one minute, expressed in µmol mol^{-1}

[b] To be discussed in future work

Formatted: Font color: Text 1, Superscript

Formatted: Font color: Text 1, Superscript

Formatted: Position:Horizontal: 0.85", Relative to: Page, Vertical: -0.25", Relative to: Paragraph, Horizontal: 0.13", Height: Exactly 0.5", Wrap Around

Formatted: Font color: Text 1

Formatted: Font color: Text 1

Formatted: Font:9 pt, Bold, Font color: Text 1, Superscript

Formatted: Font:9 pt, Bold, Font color: Text 1

2.2.1 Trace Gases

Greenhouse gases

Continuous measurement of CO_2, CO, CH_4 and N_2O were made using a high precision FTIR trace gas and isotope Spectronus analyser, developed by the Centre for Atmospheric Chemistry at the University of Wollongong. The analyser combines a Fourier Transform Infrared (FTIR) Spectrometer (Bruker IRcube), a pressure and temperature controlled multi-pass cell and an electronically cooled mercury cadmium telluride detector. A detailed description of the instrument and concentration retrieval technique are available in Griffith et al. (2012) and Griffith (1996).

Ozone and other trace gases

A Multi Axis Differential Optical Absorption Spectrometer (MAX-DOAS) was installed on the top of one of the laboratories during the campaign. The technique has been shown to provide the vertical profile of nitrogen dioxide, ozone, sulfur dioxide, formaldehyde, glyoxal and aerosol extinction (Sinreich et al., 2005;Honninger et al., 2004). The MAX-DOAS instrument used in this campaign was designed and built at the University of Wollongong. It consists of a vertically rotating prism capturing scattered solar radiation at different angles (1°, 2°, 4°, 8°, 16°, 30° and a reference at 90°) into a fibre optic that carries the radiation to a UV-Visible spectrometer (AvaSpec – ULS3648). Furthermore, a Thermo Scientific model 49i UV Photometric Ozone analyser was used to measure ozone concentrations. Several periods of elevated biomass burning emissions resulted in interferences with the 49i UV analyser and were removed from the analyses. These periods were marked with strong correlations with

Deleted: (Griffith et al., 2012) .
Formatted: Heading 2
Formatted: Font color: Text 1
Formatted: Font color: Text 1
Formatted: Font color: Text 1
Formatted: Font color: Text 1
Formatted: Font color: Text 1
Formatted: Font color: Text 1
Formatted: Font color: Text 1
Formatted: Font color: Text 1

high concentrations of acetonitrile where other UV-absorbing species, such as certain PAH species.

Non-methane organic compounds

Online NMOC measurements were made using a high sensitivity Proton Transfer Reaction-Mass Spectrometer (PTR-MS; Ionicon Analytik) using H_3O^+ as the primary ion. The inlet was 10 m in length and drew air at 5 L min^{-1} from 2 m above the roof (approx 5.5 m above ground level). The PTR-MS ran with inlet and drift tube temperature of 60 ºC, 600 V drift tube, and 2.2 mbar drift tube pressure, which equates to an energy field of 135 Td. The PTR-MS sequentially scanned masses 15-190, with 1 second dwell time. The PTR-MS operated with the aid of auxiliary equipment which regulates the flow of air in the sample inlet and controls whether the PTR-MS is sampling ambient or zero air or calibration gas (Galbally et al., 2007).

Furthermore, AT VOC (adsorbent tube Volatile Organic Compounds) samples were collected by an automatic VOC sequencer which actively draws air through two multi-adsorbent tubes in series (Markes Carbograph 1TD / Carbopack X). The adsorbent tubes were then analysed by a PerkinElmer TurboMatrix™ 650 ATD (Automated Thermal Desorber) and a Hewlett Packard 6890A gas chromatography (GC) equipped with a Flame Ionization Detector (FID) and a Mass Selective Detector (MSD) at CSIRO Oceans and Atmosphere laboratories. Further details of the sampling and analyses are given in Cheng et al. (2016).

During sampling, carbonyls and dicarbonyls were trapped on S10 Supelco cartridges, containing high-purity silica adsorbent coated with 2,4-dinitrophenylhydrazine (DPNH), where they were converted to the hydrazone derivatives. Samples were

Comment [MM15]: R3:
6. In some cases (e.g., non methane organic compounds), too much detail is provided in the methods section describing the measurement.

Deleted:

Formatted: Font color: Text 1, Subscript

Formatted: Font color: Text 1

Deleted: During the campaign the PTR-MS was calibrated once per day for the following compounds using certified gas standards from Apel Riemer Environmental Inc, USA and Air Liquide Specialty Gases, USA: acetaldehyde, acetone, acetonitrile, benzene, methacrolein, methanol, methyl ethyl ketone, toluene, 1,3,5-trimethyl benzene, m-xylene, chlorobenzene, alpha pinene, 1,2-dichlorobenzene, 1,3,4 trichlorobenzene, dimethyl sulphide and isoprene. Calibration data were used to construct sensitivity plots, which were used to calculate approximate response factors for other masses not specifically calibrated.

Formatted: Font color: Text 1

Formatted: Font color: Text 1

Deleted: NP

Formatted: Font color: Text 1

Formatted: Font color: Text 1

refrigerated immediately after sampling until analysis. The derivatives were extracted from the cartridge in 2.5 mL of acetonitrile and analysed by high performance liquid chromatography with diode array detection. The diode array detection enables the absorption spectra of each peak to be determined. The difference in the spectra highlights which peaks in the chromatograms are mono- or dicarbonyl DNPH derivatives and, along with retention times, allows the identification of the dicarbonyls glyoxal and methylglyoxal. Further details can be found in Lawson et al. (2015).

Formatted: Font color: Text 1

Formatted: Font color: Text 1

PAHs

PAHs were sampled through a high-volume air sampler (Kimoto Electric Co., LTD.) using a sampling rate typically at ~60 m^{-3} h^{-1}. The sampling rate was calibrated using an orifice plate prior to the sampling campaign and the sampling volume was calculated based on the calibrated sampling rate and sampling duration. A bypass gas meter installed on the sampler was used to monitor any anomalous fluctuation of the sampling rate during the sampling period. Particle-associated and gaseous PAHs were collected on glass fibre filters (Whatman™, 203×254 mm, grade GF/A in sheets) and subsequent polyurethane foam plugs respectively. The glass fibre filters and polyurethane foam, along with the field blank samples, were extracted separately using an Accelerated Solvent Extractor (Thermo Scientific™ Dionex™ ASE™ 350) after being spiked with a solution containing 7 deuterated PAHs (i.e. $^{2}D_{10}$-phenanthrene, $^{2}D_{10}$-fluoranthene, $^{2}D_{12}$-chrysene, $^{2}D_{12}$-benzo[b]fluoranthene, $^{2}D_{12}$-BaP, $^{2}D_{12}$-indeno[1,2,3-cd]pyrene, $^{2}D_{12}$-benzo[g,h,i]perylene) at different levels as internal standards for quantification purposes. Concentrated extracts were cleaned up by neutral alumina and neutral silica. Eluents were carefully evaporated to near dryness and refilled with 250 pg of $^{13}C_{12}$-PCB (polychlorinated biphenyl) 141 (in 25 µL isooctane) employed as the recovery/instrument standard for estimating the recoveries of the spiked internal

standards and monitoring the performance of the analytical instrument. Samples were analysed using a Thermo Scientific™ TRACE™ 1310 gas chromatograph coupled to a Thermo Scientific™ double-focusing system™ Magnetic Sector high resolution mass spectrometer. The HRMS was operated in electron impact-multiple ion detection mode and resolution was set to ≥ 10,000 (10% valley definition). An isotopic dilution method was used to quantify 13 PAH analytes including phenanthrene, anthracene, fluoranthene, pyrene, benzo[a]anthrancene, chrysene, benzo[b]fluoranthene, benzo[k]fluoranthene, benzo[e]pyrene, BaP, indeno[1,2,3-cd]pyrene, dibenzo[a,h]anthracene, benzo[g,h,i]perylene.

Mercury

Total gaseous mercury, gaseous elemental mercury + gaseous oxidised mercury (TGM; GEM + GOM), was sampled from a 10 m mast and measured via gold pre-concentration and cold vapour atomic fluorescence spectroscopy using a Tekran 2537X instrument. Simultaneously, GEM, GOM and Particulate-bound mercury (PBM) were individually measured using a Tekran 2537B connected to a combined Tekran 1130/1135 speciation unit sampling at a 5.4 m height. The sampling train of the 1130/1135 collects first GOM (KCl-coated denuder) then PBM (quartz wool pyrolyser) in series from a 10 L min^{-1} sampling flow, allowing GEM only to flow onwards for detection by subsampling by the 2537B. Due to the small atmospheric concentrations of GOM and PBM, pre-concentration occurred over a 1-hour period with subsequent analysis taking an additional hour. Continuous measurements of GEM at 5-minute resolution were made possible for the 2537B unit by rotating pre-concentration/analysis roles of the two internal gold traps. Both 2537 units sampled at 1 L min^{-1} and were calibrated every 23 hours using an internal mercury permeation source. For more information on the 2537 and 1130/1135 systems see Landis et al. (2002) and Steffen et al. (2008).

Formatted: Font color: Text 1

Formatted: Font color: Text 1

Comment [MM17]: R1:
Line 241. The term PBM need to be defined here.

Formatted: Font color: Text 1

Deleted:

Formatted: Font color: Text 1

Formatted: Font color: Text 1

Formatted: Font color: Text 1

Formatted: Font color: Text 1

GEM fluxes were measured using the methods outlined in Edwards et al. (2005). Air samples were drawn at heights of 5.2 and 8.0 m through 46.4 m of nylon tubing using a PTFE diaphragm pump operating at 10 L min^{-1}. Subsampling from this flow through a 0.2 µm PTFE filter at 1 L min^{-1} by a Tekran 2537A, and switching between sample intakes, allowed resolution of a GEM gradient every 30 minutes. The transfer velocity was measured using a Campbell Scientific CSAT3 sonic anemometer and LI-COR 7200 closed path infrared gas analyser for CO_2, both located on the same tower as the gradient intakes at 6.6 m and sampling at 20 Hz.

Formatted: Font color: Text 1

Formatted: Font color: Text 1

Radon

In order to measure Radon concentrations, a 700 L dual-flow-loop two-filter radon detector, designed and built by the Australian Nuclear Science and Technology Organisation (Whittlestone and Zahorowski, 1998;Chambers et al., 2014), was installed at the ATARS in 2011 and has been fully operational since July 2012. The detector provided continuous hourly radon concentrations for the duration of the SAFIRED campaign, sampling air at 40 L min^{-1} from 12 m above ground level through 25 mm high-density polyethylene agricultural pipe. A coarse aerosol filter and dehumidifier were installed "upstream" of the detector, as well as a 400 L delay volume to ensure that thoron (^{220}Rn, half-life 55 s) concentrations in the inlet air stream were reduced to less than 0.5 % of their ambient values. The detector's response time is around 45 minutes, and the lower limit of detection is 40 - 50 mBq m^{-3}. Calibrations are performed on a monthly basis by injecting radon from a PYLON 101.15±4% kBq Ra-226 source (12.745 Bq min^{-1} ^{222}Rn), traceable to NIST standards, and instrumental background is checked every 3 months. In post processing, half-hourly raw counts were integrated to hourly values before calibration to activity concentrations (Bq m^{-3}).

Comment [MM18]: R2:
The Radon instrument description also includes a summary of how Radon measure- ments are used in atmospheric research. This is not appropriate here and should be moved to the results section around page 21.

Formatted: Font:Not Bold, Font color: Text 1

Formatted: Font color: Text 1

Formatted: Heading 3

Deleted: . ... [37]

Formatted: Font color: Text 1

Formatted: Font color: Text 1

Formatted: Font color: Text 1

Formatted: Font color: Text 1

Formatted: Font color: Text 1

2.2.2 Aerosols

Aerosol Drying System

An Automated Regenerating Aerosol Diffusion Dryer (ARADD) is permanently installed on the roof of the laboratory containing the aerosol instrumentation for this campaign. This was used in front of the aerosol manifold to continuously dry the aerosol sample. The ARADD design, similar to that described by Tuch et al. (2009), continuously conditions the aerosol sample to a relative humidity of below 40% with maximum aerosol transmission efficiency. The ARADD utilizes two diffusion drying columns in parallel, each containing 7 stainless steel mesh tubes of 10 mm internal diameter and approximately 800 mm length, surrounded by a cavity packed with silica gel. The aerosol sampled is directed into one column at a time, while the other column is regenerated by an ultra-dry compressed air system. All flows are controlled by software that directs sample flow and compressed air flow to the appropriate column with a series of valves. The ARADD has total suspended particulate style intake at the inlet of the aerosol sample path. This is a non-size-selective stainless-steel inlet with a semi-cicular hat over an inverted conical funnel of variable pitch ending with a 3/4" stainless-steel tube. In practise, the aerosols collected have an equivalent aerodynamic diameter of 100 µm or less depending on sampling conditions. The inlet led to a sample manifold at the exit of the system to provide sampling take-offs for the various aerosol instruments connected to the ARADD. Flow through the ARADD is provided by the instruments and pumps connected downstream. The ambient and inlet relative humidity for the entire sampling period were logged and are displayed in Supplementary Figure S1.

Comment [MM21]: R2:
The chapter Aerosols should be numbered consistently with 2.2.2

Formatted: Font color: Text 1

Formatted: Font color: Text 1

Formatted: Font color: Text 1

Formatted: Font color: Text 1

Comment [MM22]: R1:
Line 307. What is a 'Total Suspended Particulate style inlet'? I've never heard of this, so it needs to be explained further or a reference given that explains it.

Deleted: a T

Deleted: S

Formatted: Font color: Text 1

Deleted: P

Formatted: Font color: Text 1

Formatted: Font color: Text 1

Formatted: Font color: Text 1

Deleted: , and a

Formatted: Font color: Text 1

Formatted: Font color: Text 1

406 **Aerosol Size**

407 Aerosol size distributions were measured with a Scanning Mobility Particle Sizer
408 (SMPS). A TSI 3071 long-column electrostatic classifier with a TSI 3772 Condensation
409 Particle Counter (CPC) measured the size distribution over a range of 14 nm to 670 nm
410 at a scan interval of 5 minutes.

411

412 In addition to the aerosol size distributions measured by the SMPS, neutral and charged
413 aerosol particle distributions from 0.8 nm to 42 nm were measured using a Neutral
414 cluster and Air Ion Spectrometer (NAIS)(Manninen et al., 2009;Mirme et al., 2007). In
415 this study, the NAIS was set to operate in a cycle of 4 min including ion and neutral
416 particle sampling periods of 2 and 1 minute, respectively, with the remaining minute
417 being an offset period which is required to neutralize and relax the electrodes. The total
418 sampling air flow was 60 L min^{-1}, the high flow rate being used to minimize ion
419 diffusion losses and maximize the measured ion concentration sensitivity. Ion losses
420 are accounted for during post-processing of the data by the software (Mirme et al.,
421 2007).

422 **Aerosol Composition and Water Uptake**

423 PM_1 and PM_{10} 12-hour filter samples (night and day) were collected on a TAPI 602
424 Beta plus particle measurement system (BAM). Portions of the PM_1 filters have been
425 analysed for elemental and organic carbon mass loadings using a DRI Model 2001A
426 Thermal-Optical Carbon Analyzer following the IMPROVE-A temperature protocol
427 (Chow et al., 2007b). Additional portions of the PM_1 filters were extracted in 5 ml of
428 18.2 mΩ de-ionized water and preserved using 1% chloroform. These extracts have
429 been analysed for major water-soluble ions by suppressed ion chromatography and for

Formatted: Font color: Text 1
Formatted: Font color: Text 1
Formatted: Font color: Text 1
Formatted: Font color: Text 1
Formatted: Font color: Text 1
Formatted: Font color: Text 1
Deleted: will be
Formatted: Font color: Text 1

anhydrous sugars including levoglucosan by high-performance anion-exchange chromatography with pulsed amperometric detection (Iinuma et al., 2009).

Daily aerosol filters were collected using two Ecotech 3000 high-volume volumetric flow controlled aerosol samplers with PM_{10} size selective inlets. One high-volume sampler was used to collect aerosols on acid cleaned Whatman 41 filters to determine the soluble and total fraction of trace metals. Soluble trace metals were extracted from a filter aliquot using ultra-pure water (>18.2 mΩ) leaching experiments. Total trace metal concentrations were determined by digesting a second filter aliquot with concentrated nitric and hydrofluoric acids. Leachates and digested solutions were analysed by high resolution inductively couple plasma mass spectrometry. The second sampler was used to collect a set of aerosol samples on quartz filters for elemental and organic carbon analysis following (Chow et al., 2007a), and major anion and cation analysis.

The volatility and hygroscopicity of 50 nm and 150 nm particles were measured with a custom built Volatility and Hygroscopicity Tandem Differential Mobility Analyser (VH-TDMA). Inlet dried particles were size selected (alternating between 50 and 150 nm) using a TSI 3080 electrostatic classifier. Scans alternated between two different sample pathways. In the first, after size selection, particles were passed through a thermodenuder set to 120°C. The sample line was then split so that half went to an SMPS comprised of a TSI 3080 classifier and a TSI 3010 CPC (V-TDMA). The rest of the sample was passed through a humidifying system that exposed the particles to a relative humidity of 90% before being brought into another SMPS with a 3080 classifier and 3010 CPC (H-TDMA). Alternatively, the thermodenuder was bypassed in every

Comment [MM23]: Line 335. Are you saying that the extracts have not been analyzed yet?

Formatted: Font color: Text 1

Formatted: Font color: Text 1

Formatted: Font color: Text 1

Formatted: Font color: Text 1

Formatted: Font color: Text 1

second scan so that the V-TDMA was used to verify the size selection and the H-TDMA was able to observe the hygroscopic growth of ambient particles. Each scan ran for 3 minutes, giving a full set of data every 12 minutes.

The chemical composition and properties of non-refractory sub-micron particles were investigated with a compact Time-of-Flight Aerosol Mass Spectrometer (cToF-AMS, Aerodyne Research, Inc.) and a Time of Flight Aerosol Chemical Speciation Monitor (ToF-ACSM, Aerodyne Research, Inc.). Both of these instruments operate with the same principle and have many identical components. An aerodynamic lens in the inlet of each instrument focuses the particles into a beam and differential pumping removes most of the gas phase. Particles are flash vaporized at 600°C and ionized by electron impact before passing through a time-of-flight mass spectrometer to a multi-channel plate detector in the cToF-AMS and a dynode detector in the ToF-ACSM. The cToF-AMS has the added benefit of having a particle Time-of-Flight (pToF) mode, which allows the size resolved chemical composition to be measured. Both instruments sampled through a $PM_{2.5}$ inlet and nafion dryer. In addition, the inlet of the cToF-AMS was incorporated into the VH-TDMA system, so that when the VH-TDMA was measuring ambient particles, the cToF-AMS would draw particles through the thermodenuder set at 120°C and vice-versa. This gives additional information about the chemical composition of the volatile component of submicron particles.

The number of particles activated to cloud droplets were measured using a Continuous-Flow Steam Wise Thermal Gradient Cloud Condensation Nuclei Counter (CCNC) from Droplet Measurement Technologies Inc. (DMT, model No. 100). Particles were

exposed to a 0.5% supersaturation and activated particles greater than 1µm were counted with an Optical Particle Counter using a 50 mW, 658 nm laser diode.

Back trajectories

Hourly 10-day air mass back trajectories terminating at ATARS were produced using the NOAA HYSPLIT model (Draxler and Rolph, 2003), and catalogued in a data base for use with the SAFIRED campaign data set. Global Data Assimilation System input files with 0.5° resolution were obtained from NOAA ARL FTP site (http://ready.arl.noaa.gov/gdas1.php) to drive the HYSPLIT model.

Satellite detection of fires

Data on the location of fires was collected from the Australian national bushfire monitoring system, Sentinel Hotspots. Hotspot locations are derived from the Moderate Resolution Imaging Spectroradiometer (MODIS) sensors on the Terra and Aqua satellites and the Visible Infrared Imaging Radiometer Suite (VIIRS) sensor on the Suomi NPP satellite. The Terra, Aqua and Suomi NPP satellites fly over the region around ATARS at approximately 10:30 am, 3 pm and 2:30 pm, respectively. Detection of fires is therefore limited to those that are flaming during these times.

Formatted: Font color: Text 1

Formatted: Font color: Text 1

Formatted: Default Paragraph Font, Font color: Text 1

Formatted: Font color: Text 1

3. Overview of Campaign

Fires and air masses

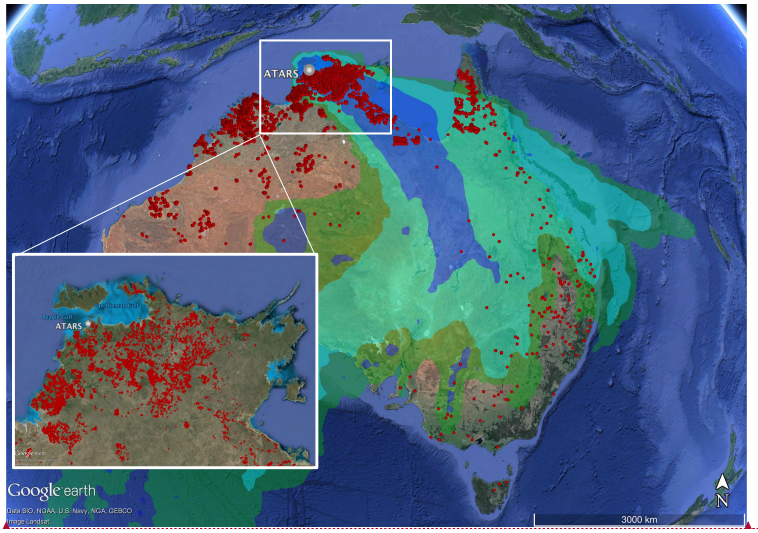

Figure 1 All satellite-detected fires with >50% detection confidence in June 2014 in Australia. Trajectory densities are shown as shaded regions (blue - >10% of all data; cyan - >1% of all data; green - >0.1% of all data).

Thousands of fires were observed in during the period of the SAFIRED campaign in Australia by the MODIS and VIIRS sensors on the Terra and Aqua NASA satellites. The vast majority of these occurred in the savannah regions of northern Australia. Over 28000 fires were detected within 400 km of ATARS during the sampling period. . Airmass back trajectories from the sampling site show that air masses over the study period predominately originated from the southeast (see Figure 1), generally over the regions where fires were frequently detected. Considering the daily satellite observations of close and distant fires, as well as meteorological, gaseous and aerosol measurements over the duration of SAFIRED, five periods were distinguished; four biomass burning related periods (BBP1, BBP2, BBP3 and BBP4) and a "coastal" period (CP). The dates for these periods are displayed in Table 2.

Comment [MM24]: R3:
1. The resolution of the figures is too poor and needs to be fixed. I would ask the authors to consider using vector images.
2. The font size on the figures in some cases is too small and very hard to discern on a printed copy of the manuscript.

Formatted: Font color: Text 1

Comment [MM25]: R2:

What I was mostly missing in this chapter was putting SAFIRED into the bigger picture of fire emissions in Australia, e.g.: how representative is SAFIRED, was this a typical year and what could SAFIRED potentially tell us about emission estimates in northern Australia. How many fires did you observe during SAFIRED? How many of those measured plumes were fresh (for emission ratios) and how many were aged?

Formatted: Heading 2

Formatted: Font color: Text 1

Formatted: Font color: Text 1

Formatted: Font color: Text 1

Formatted: Centered

Deleted: **The HYSPLIT (a) back and (b) forward trajectories to and from the ATARS site, truncated to five days. The colour scale represents the air mass trajectory density, normalised to 1. Grey dots are MODIS and VIIRS detected hotspots from the 30th of May 2016 until the 29th of June 2016.**

Formatted: Font color: Text 1

Formatted: Font color: Text 1

Deleted: (Figure 1)

Table 2 The start and end dates for the four identified Biomass Burning Periods (BBP1, BBP2, BBP3 and BBP4) and the Coastal Period (CP).

Period	Start date (mm/dd/yy hh:mm)	End date (mm/dd/yy hh:mm)
BBP1	05/30/14 00:00	05/31/14 23:59
BBP2	06/06/14 00:00	06/12/14 23:59
BBP3	06/14/14 00:00	06/17/14 23:59
CP	06/19/14 12:00	06/22/14 23:59
BBP4	06/23/14 00:00	06/28/14 23:59

The number of detected fires on each day within 10 km, 20 km, 50 km, 100 km and 200 km of the sampling location was determined (see Figure 2). Several fires within 10 km were detected on the 30th of May (BBP1), the 9th and 10th of June (BBP2) and the 25th and 26th of June (BBP4). BBP1, BBP2 and BBP4 were also associated with the highest concentrations of most of the measured gaseous (Figure 3) and aerosol species (Figure 4). The periods between the 12th and 23rd of June (BBP3 and CP) had very few detected fires within 50 km of the station, corresponding to smaller gaseous and aerosol concentrations.

Deleted: The number of detected fires on each day within 10 km, 20 km, 50 km, 100 km and 200 km of the sampling location was determined (Figure 2). Several fires within 10km were detected on the 30th of May and the 9th, 10th, 25th and the 26th of June. These correspond with the highest gaseous and aerosol signals. The periods between the 11th and 24th of June had very few detected fires within 50km of the station. Satellite flyby times were in the early afternoon local time each day and therefore fires not occuring during these times would not be recorded. Airmass back trajectories from the ATARS site show that air masses over the study period were predominately southeasterly (Figures 1a and 4c), generally over the regions where fires were frequently detected.

Formatted: Font color: Text 1

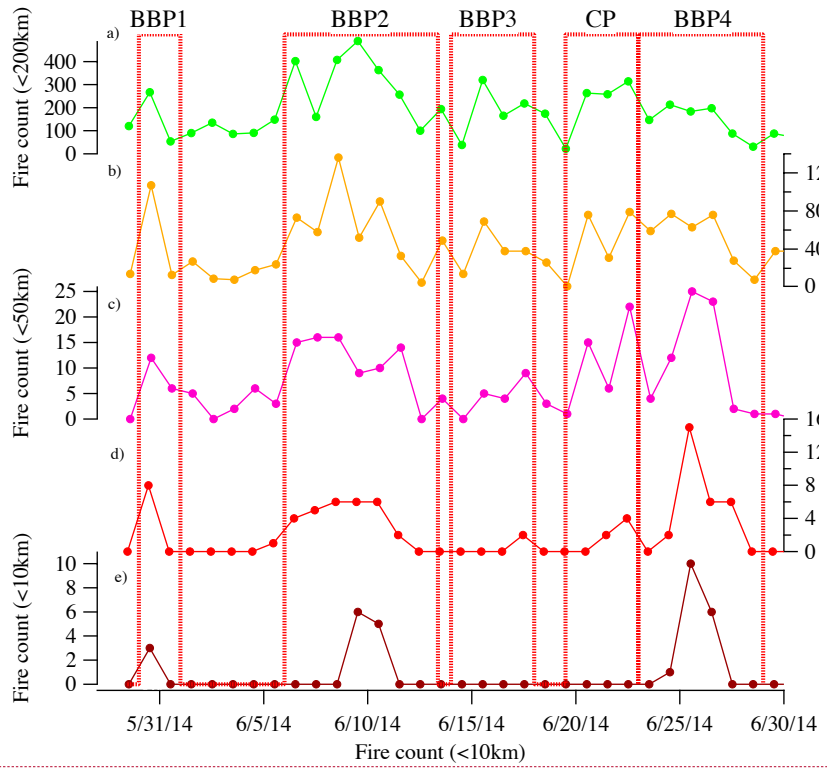

Figure 2 The number of hotspots observed each day within (a) 200 km, (b) 100 km, (c) 50 km, (d) 20 km and (e) 10 km of the ATARS, as detected by the MODIS and VIIRS sensors on the Terra and Aqua satellites.

Formatted: Font color: Text 1

Formatted: Font color: Text 1

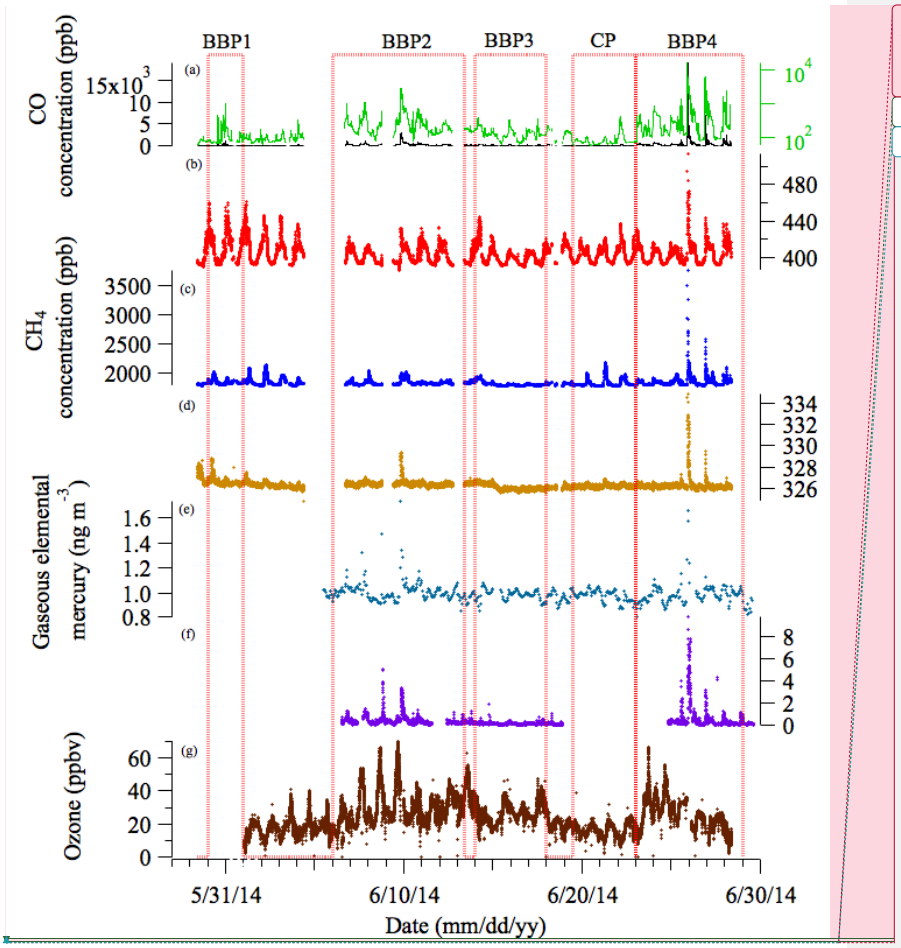

549

550 **Figure 3 The time series of the major measured gaseous species during the SAFIRED campaign: (a) carbon**
551 **monoxide, (b) carbon dioxide, (c) methane, (d) nitrous oxide, (e) gaseous elemental mercury, (f) acetonitrile**
552 **and (g) ozone. The biomass burning and coastal periods are indicated by the red dotted lines. All parts-per**
553 **notation refer to mole fractions unless otherwise indicated. The date and time is local time.**

Comment [MM26]: R2:
Figures 5 and 8. It would be good to also show the CO data on a linear scale.

Moved (insertion) [1]

Formatted: Font color: Text 1

Comment [MM27]: R1:
Figure 5 Caption. Plot (d) is mistakenly attributed to 'nitrogen dioxide' and should be nitrous oxide.

Deleted: gen

Deleted: di

Deleted: and $\Delta O_3/\Delta CO$

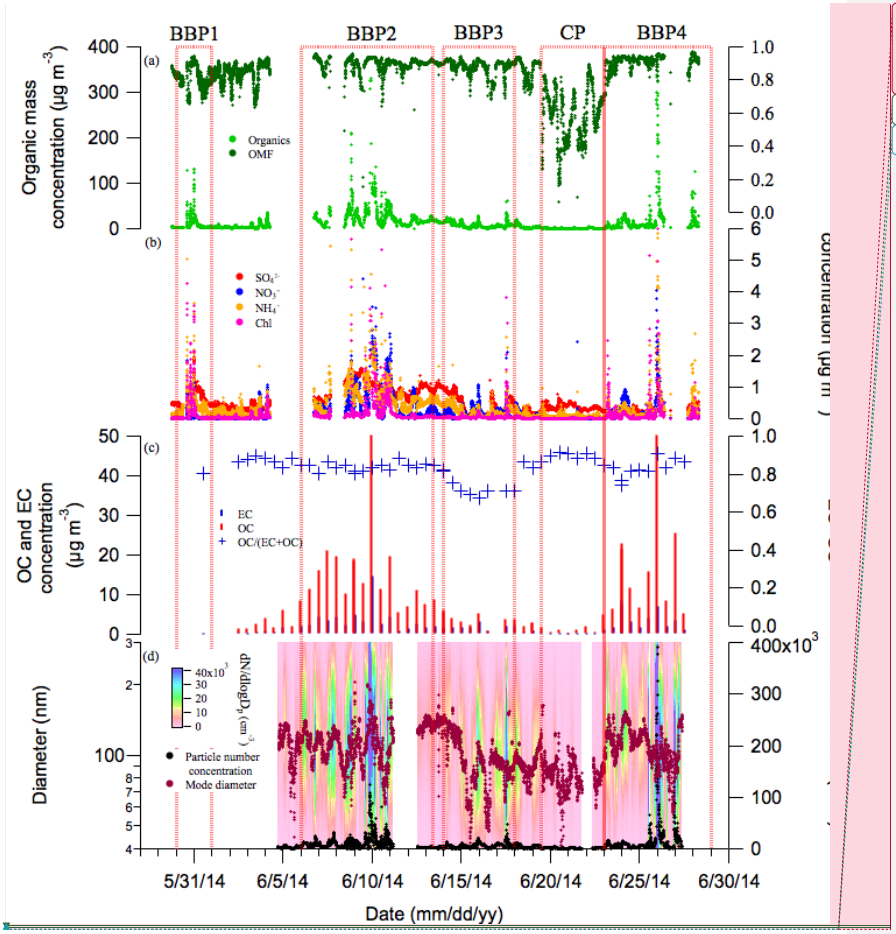

Figure 4 The times series of the major aerosol properties during the SAFIRED campaign: (a) the non-refractory PM_1 organic mass concentration (left) and organic mass fraction (right), b) the inorganic non-refractory PM_1 mass concentrations, (c) the 12-hour filter OC and EC PM_1 mass concentrations (left) and the ratio of OC to OC+EC (right), (d) the particle size distributions and particle size mode (left) and the total particle number concentration (right) and (e) the wind direction at ATARS. The date and time is local time.

Most of the gaseous and aerosol time series show a pronounced diurnal trend, with higher concentrations typically observed during the night (see Figure 5 and Supplementary Figure and S2). This is likely due to a combination of variations in fire locations, time of burns, and changes in the boundary layer height or wind velocity. The diurnals trends of radon concentrations, temperature, wind speed, wind direction and greenhouse gases for each of the BBPs and the CP are displayed in Figure 5. The

Comment [MM28]: Figure 6. The legends and scale insets are too small and, in one case, not next to the panel to which they refer.

Moved (insertion) [2]

Formatted: Font color: Text 1

Formatted: Caption

Deleted: ... [38]

radon concentrations provide further information regarding the regional air mass origins and the degree of contact with the land surface and give insight into the boundary layer. Sharp decreases in the radon concentrations were observed after 09:00 local time and did not increase until after sunset at approximately 18:00 for all periods (Figure 5a), suggesting a pronounced diurnal variation in the boundary layer height. Furthermore, radon concentrations were consistently lower during the CP than the BB periods, suggesting less terrestrial influence than the rest of the sampling period. The HYSPLIT air mass back trajectory for the CP originated along the east coast of Australia and passing over little land before arriving at the station. Figure 5d supports this, showing predominately easterly and northeasterly winds during the night and day, respectively. The diurnal variations during the BB periods were more pronounced. The winds during these periods were predominately southeasterly during the night and morning, turning easterly during the afternoon before reverting at approximately 20:00 local time. The HYSPLIT air mass back trajectories for the BB periods indicated terrestrial origins, with air masses passing predominately over the savannah region of northern Australia where the fires occurred.

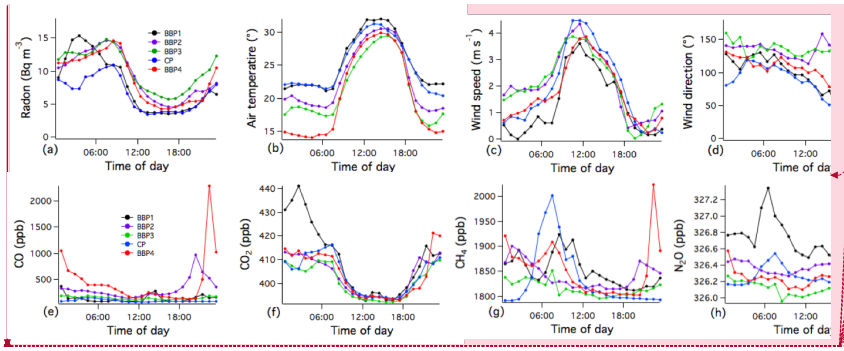

Figure 5 Mean hourly diurnal (a) radon, (b) wind speed, (c) wind direction, (d) dew point temperature (e) CO, (c) CO_2, (d) CH_4, and (e) N_2O at ATARS, separated into different biomass burning periods (BBP) and a coastal period (CP)

Comment [MM30]: R2:
Figure 4c y-axis should go from 0-360.

Comment [MM31]: R2:
Figure 4: The data here are split into weak moderate and strong mixing, but nothing is really done with this separation later. Also the differences are not very strong. In the next Figure and the rest of the manuscript the data get separated into different BB and costal periods. This seems a better separation. I suggest removing the mixing categories. I am also wondering how the wind direction plot looks for the Coastal Period. This would be more helpful for a separation.

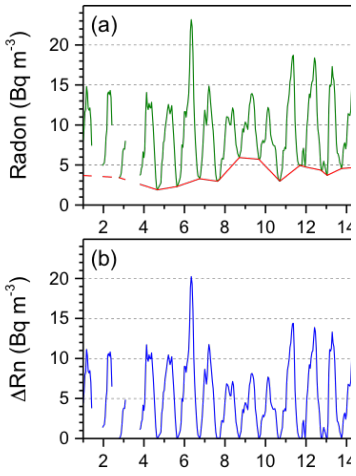

Deleted: ... [39]

Formatted: Font color: Text 1

Formatted: Font color: Text 1

Formatted: Font color: Text 1

Formatted: Font color: Text 1

Formatted: Centered

Formatted: Font color: Text 1

Formatted: Font color: Text 1

Formatted: Font color: Text 1

Formatted: Font color: Text 1

Formatted: Font color: Text 1

Deleted: 4

Deleted: composite

Deleted: , and

Formatted: Font color: Text 1

Formatted: Font color: Text 1

Formatted: Font color: Text 1

Formatted: Font color: Text 1

With numerous fires occurring across the region and the limitations of once-per-day satellite fly-overs and stationary measurements, it can be difficult to identify the exact source of these elevated signals. Nonetheless, it is possible to link detected plumes with fires given back trajectory analysis. The elevated signals during BBP1 were likely a result of several fires that were burning and observed on the 30th of May at 14:00 local time approximately 2 and 10 km from ATARS during the day. While the elevated signals were observed later in the evening, it is likely that they were due to a continuation or evolution of those fires. Some of the most intense signals of the campaign were observed during BBP2, with numerous close (within 50 km) and distant (within 200 km) detected. Due to the limitations of the once-per-day satellite fly-by, it was only possible to link one of the observed plumes to a source during this period. A large event observed on the evening of the 9th of June was likely due to a cluster of fires detected approximately 5 km southeast of ATARS. Only one fire within 20 km of ATARS was observed via satellite during BBP3 on the 17th of June but this was not associated with any significant increase in gaseous or aerosol concentrations. Several fires were also observed between 20 km and 50 km from the station. One close fire was also observed during CP, however wind directions during this period were typically north-easterly and concentrations were therefore much lower. 5-day HYSPLIT trajectories also show that air mass during the CP originated along the east coast of Australia before travelling towards the sampling station with very little terrestrial influence.

For a portion of BBP4, fires were burning within several kilometers of ATARS and several plumes were easily observed from the station. The signals from these plumes are shown in Figure 6. The observed enhancements between 12:30 and 15:00 pm on

Deleted: at ATARS, as a function of radon-based nocturnal mixing categories.

Formatted: Font color: Auto

the 25th June during BBP4 were a result of grass fires burning approximately 2 km south-east from the station. During this event, the wind direction was highly variable, changing between 140° and 80° True Bearing (TB) multiple times. As a result, the sampling changed from measuring the air mass with and without the plume from this fire, which led to sharp increases and decreases in biomass burning-related signals. Visually, the fire area and extent of the plume was larger at 4:00pm than earlier, however the wind direction changed to north-easterly which directed the plume away from the station. From 16:00 until 22:00, the wind direction was stable at approximately 50° TB. At 22:00, the wind direction rapidly changed to directly south and the largest enhancements for the whole campaign were observed until approximately 2:00 am on the 26th of June. It is very likely that these signals were a result of a continuation and evolution of these fires as the night progressed. Portions of a ~0.25 km^2 grassland field within 500 m directly south of ATARS were observed to be burned upon arrival at the station on the morning of the 26th of June and we speculate that the burning of this field contributed to the large enhancements in measured biomass burning emissions. The emissions during this portion of BBP4 are likely to be the most representative of fresh biomass burning smoke during the SAFIRED campaign. Significant ozone enhancements over 80 ppb were observed during this event, although this was likely result of a cross-contamination due to concurrently high concentrations of UV-absorbing organic compounds in the gaseous phase. This enhancement would only be possible with significant photochemical processing which is very unlikely considering the time of the event, the visual evidence of close fires, and the large concentrations observed.

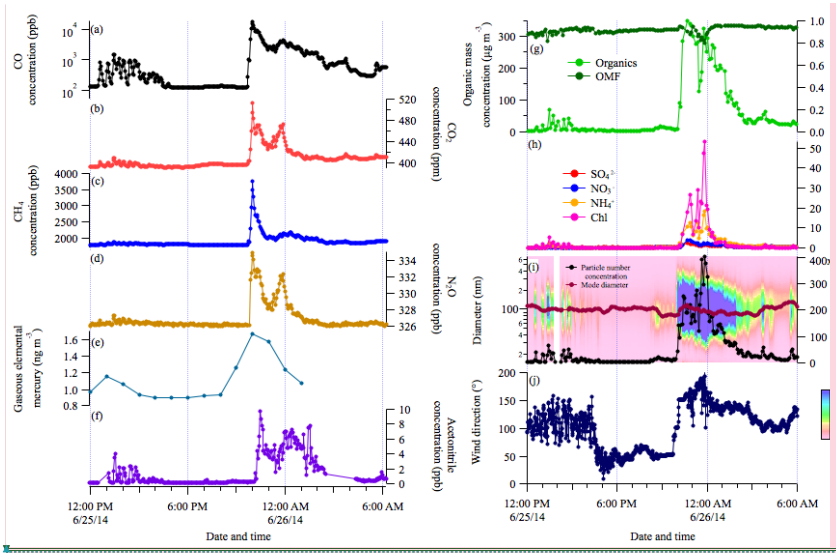

Figure 6. The major gas and aerosol concentrations measured during two biomass burning events within 1 km of ATARS during BBP4. (a) through (g) and (h) through (k) are as per Figures 3 and 4, respectively. All parts-per notation or mole fractions unless otherwise indicated. The date and time are local time.

Based on the elevated concentrations of biomass burning related gaseous and aerosol species, detection of close fires and the air mass back trajectory analysis during portions of BBP1, BBP2 and BBP4, these periods are likely associated with fresh biomass burning smoke from nearby fires. With smaller concentrations and more distant observed fires, the signals observed during BBP3 are possibly more characteristic of aged biomass burning smoke. The influence of biomass burning during CP was much smaller than the rest of the campaign. Investigating the relationship between toluene and acetonitrile, two NMOCs emitted from biomass burning, can provide further information on the aging of BB emissions. Toluene is much shorter lived than acetonitrile as it readily reacts in the presence of the OH radical. Assuming a consistent emission ratio of these two NMOCs from fires in this region, the ratio of toluene/acetonitrile thereby provides a proxy for photochemical age. Unfortunately, the PTR-MS which measures these species was not operational during BBP1 and CP. The

Comment [MM32]: R2:
The ozone enhancement shown in Figure 8 for the close proximity fire is substan- tial and ozone values of almost 100ppb are detected in the plume. This means that there has been significant photochemical processing of potentially several hours dur- ing plume transport. If the plume would be really fresh, ozone would actually be titrated. Again VOC/CO could be very helpful here and should be looked into. Also a compar- ison to a nighttime plume measurement would be very useful. Again, I doubt that this plume is very fresh.

Comment [MM33]: R2:
O3/CO ratios: The O3/CO is used in Figures 5 and 8 and is described at giving an indication of photochemical age. Unfortunately O3/CO are much more complicated than that and depend on many different factors such as VOC/NOx ratios such that the ratio really cannot be used as "photochemical age". I think for this paper here, it is best to remove the O3/CO ratios instead of adding a proper explanation.

Line 623. The authors seem to be ignoring the high O_3 plume during BBP4 which indicates faster O_3 production in this plume. This would seem to be one of the more interesting observations of this study.

Moved (insertion) [3]

Formatted: Font color: Text 1

Deleted: 8

Deleted: 5

Deleted: 6

diurnal trends for the toluene and acetonitrile concentrations and the toluene/acetonitrile ratio is shown in Figure 7 for BBP2, BBP3 and BBP4. The toluene/acetonitrile ratio was highest during the night, indicating more photochemically aged smoke throughout the day. Interestingly, while the toluene and acetonitrile concentrations were consistently higher during BBP2 and BBP4 than BBP3, the toluene/acetonitrile ratio was of the same magnitude and followed the same trend. It is therefore plausible that, while there were not large enhancements in concentrations during BBP3 and there were few fires detected close-by during the daytime satellite flyovers, there were small-scale burns during the night that were close enough for the emissions to reach sampling site. This observation highlights the limitation of using satellite hotspot detection in fully understanding the aging processes of biomass burning emissions.

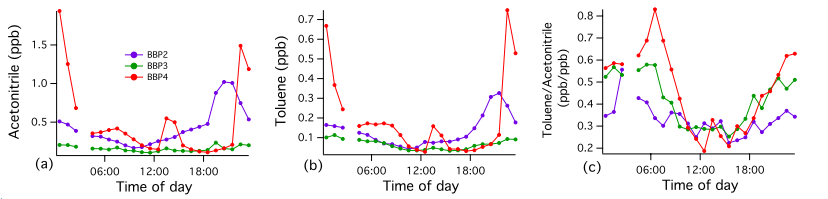

Figure 7 Mean hourly diurnal (a) acetonitrile concentration, (b) toluene concentration, (c) toluene/acetonitrile ratio, separated into different biomass burning periods (BBP).

Particle size distributions were unimodal for the majority of the sampling period with a mode of approximately 100 nm on average (see Figure 8). The SMPS was not operational during BBP1. Although the shape of the BBP4 size distribution was similar to the campaign average, concentrations were much higher and a result of close fires. BBP2 had a slightly larger size distribution centered on 110 nm. The size distribution during BBP3 was slightly smaller than the campaign average and BBP2 and BBP4,

Formatted: Font color: Text 1

Formatted: Caption

with a mode centered on ~95 nm. Furthermore, the diurnal trends of the BBA mode diameter during BBP2, BBP3 and BBP4 and CP all showed a clear maximum during the night (see Supplementary Figure S2d). The diurnal trends of the toluene/acetonitrile ratios (Figure 7c) as well as the ratio of oxygenated organic aerosol to total organics (see Supplementary Figure S2c) suggest that the larger night time particle sizes are more associated with fresh biomass burning. The contrast between these size distributions could be a result of atmospheric aging and dilution in which organic mass condenses onto or evaporates from the particle. Variations in fuel load or burning conditions could also contribute to this difference. The size and concentration of particles during the Coastal Period (CP) were much smaller than the rest of the campaign. There were two periods during CP where a bimodal size distribution was observed; one from approximately 3 pm until midnight on the 19th of June and the other between 2 pm and 6 pm on the 20th of June. The size distributions for both of these periods had a mode at approximately 20 nm and another at approximately 85 nm. Submicron sulfates made up to 32% of the total submicron non-refractory mass concentrations, as reported by the cToF-AMS from the period of midday on the 19th of June until midnight on the 22nd of June, whereas the average sulfate contribution for the rest of the campaign was approximately 8%. The low radon values, small particle concentrations, bimodal size distributions and significant contributions of sulfate during this period also suggest very little biomass burning signal and a more marine-like aerosol. No particle nucleation events were observed over the entire sampling period (See Supplementary Figure S3). This is likely due to the elevated particle concentrations acting as a condensation sink.

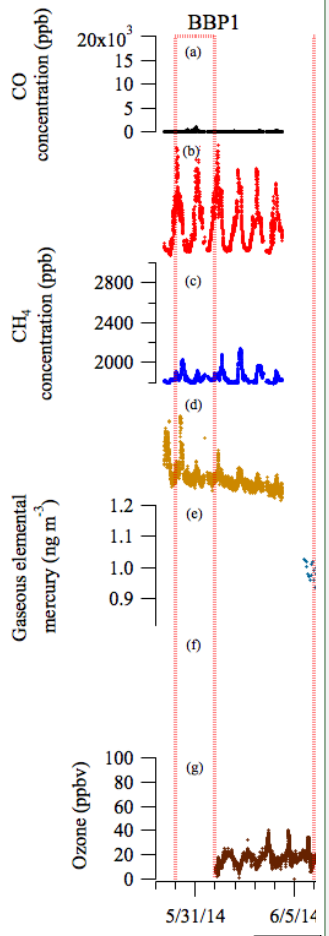

Moved up [1]: ... [45]

Formatted ... [42]

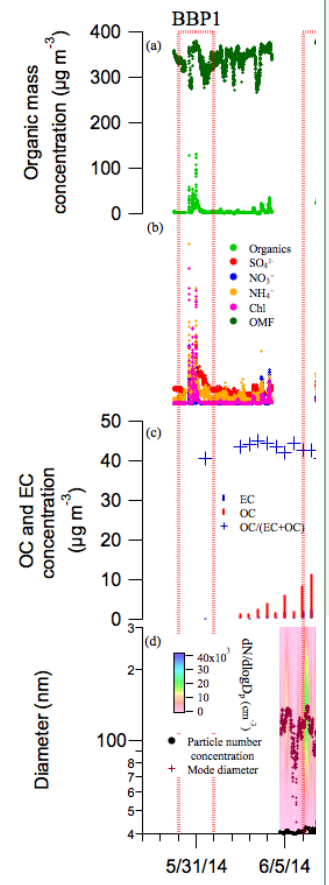

Moved up [2]: ... [47]

... [40]

Formatted ... [41]

Formatted ... [43]

Formatted ... [44]

Formatted: Font color: Text 1

Formatted ... [46]

Formatted ... [48]

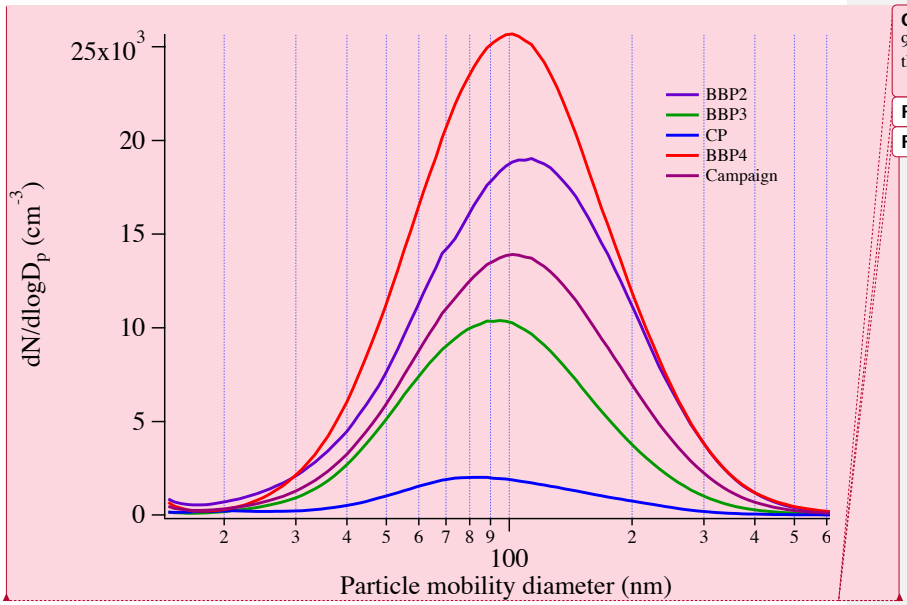

Figure 8 The average number size distribution during BBP2, BBP3, BBP4, CP and the campaign average.

Over the campaign, organics dominated the non-refectory sub-micron aerosol mass contributing, on average, 90% of the total mass. Sulphate, nitrates, ammonium and chloride species contributed the rest of this mass, with the largest contributions from sulphate and ammonium. Sulphate contributions were very significant during the coastal period, contributing up to 32% of the total mass. Although chlorides contributed the least to the total mass on average, during clear biomass burning events where sharp increases in CO and organics were observed, chlorides made up the largest component of inorganic aerosol. Organic carbon made up approximately 80% to 90% of the total carbon (organic carbon + elemental carbon) PM_1 mass during the campaign, with the exception of BBP3, when this dropped to 70%. Whether these observations were a result of burn conditions or aging processes (i.e. evaporation of organic compounds from the aerosol phase) is unclear.

Comment [MM44]: R3:
9. Figure 7: Are those raw SMPS data or lognormal fits to the SMPS data? The distributions look uncannily smooth.

Formatted: Font color: Text 1

Formatted: Font color: Text 1

Deleted: 7

Formatted: Font color: Text 1

Formatted: Font color: Text 1

Deleted: The SMPS was not operational during BBP1.

Formatted: Normal

Formatted: Subscript

Formatted: Font color: Text 1

4. Outcomes of SAFIRED

The overall aim of this study was to investigate the characteristics of BB emissions in the tropical savannah region of northern Australia during the early dry season. For many gaseous and aerosol species, elevated signals were observed for much of the month-long sampling period due to the high frequency of fires. Further analysis of these species can provide more insight into the impact of these fires on the regional atmosphere. Table 2 displays a summary of companion studies undertaken within the SAFIRED campaign.

Table 3 A list of currently published companion studies undertaken during SAFIRED.

Reference	Title
Winton et al., (2016)	Dry season aerosol iron solubility in tropical northern Australia
Wang et al., (2017)	Emissions of selected semivolatile organic chemicals from forest and savannah fires
Milic et al., (2017)	Biomass burning and biogenic aerosols in northern Australia during the SAFIRED campaign
Mallet et al., (2017)	Composition, size and cloud condensation nuclei activity of biomass burning aerosol from northern Australian savannah fires
Desservattaz et al., (2017)	Emission factors of trace gases and particles from tropical savanna fires in Australia

Deleted: BBP1, BBP2 and BBP4 correspond to the periods when fires were burning within 10 km of ATARS. Large enhancements of biomass burning related emissions were observed during these three periods. There were distinct enhancements of all measured gaseous and aerosol species during these periods. Differences between the maxir ... [49]

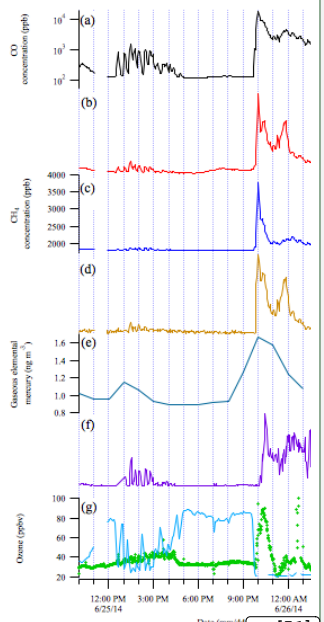

Moved up [3]: ... [51]

Formatted: Font color: Text 1

Formatted: Font color: Text 1

Deleted: (i.e. evaporation of organic compounds from the aerosol phase) is unclear, although the highest $\Delta O_3/\Delta$ ... [50]

Formatted: Font color: Text 1

Formatted: Font color: Text 1

Formatted: Font color: Text 1

Formatted: Font color: Text 1, Superscript

Formatted: Font color: Text 1

Formatted: Font:Not Bold, Font color: Text 1

Formatted: Font color: Text 1

Formatted: Font color: Text 1

Formatted: Font color: Text 1

Formatted: Font color: Text 1

Comment [MM52]: R3:
11. The 'Outcomes' section could benefit from the ... [52]

Comment [MM53]: R3:
12. Similar to comment 5, a Table listing the compa ... [53]

Formatted: Font color: Text 1

Formatted: Caption, Keep with next

Formatted Table

Howard et al., (2017)	Atmospheric mercury in the southern hemisphere tropics: seasonal and diurnal variations and influence of inter-hemispheric transport

803

804 **4.1. Emission factors and gaseous species loadings**

805 Desservettaz et al. (2017) identified individual plumes with high signals during
806 SAFIRED in order to determine emissions factors CO_2, CO, CH_4, N_2O, as well as GEM,
807 Aitken and Accumulation mode aerosols and submicron non-refractory particle species
808 (organics, sulfates, nitrates, ammonium and chlorides). Seasonal emission factors for
809 the major greenhouse gases are important for national greenhouse gas inventories and
810 in understanding the impact of savannah fires. Furthermore, these results will be the
811 first set of emission factors for aerosol particles from savannah fires in Australia, with
812 early results suggesting higher factors than those observed from African and South
813 American savannah fires. Emission factors were mostly found to be dependent on the
814 combustion conditions (using the modified combustion efficiency as a proxy) of the
815 fires.

816

817 Wang et al. (2017) investigated 13 major PAH compounds in both the gaseous and
818 aerosol phase during the SAFIRED campaign and estimated their emission factors from
819 savannah fires, as well as for subtropical eucalypt forest fires. Concentrations of these
820 PAHs varied from from ~ 1 to over 15 ng m^{-3} within different BB periods and the
821 emission factor for savannah fires for $\sum_{13}$ PAHs were estimated to be 1600 ± 110 µg
822 kg^{-1} In the gas phase, 3- and 4-ring compounds typically contributed ~ 90% to the sum
823 concentrations whereas the particle-associated PAHs were dominated by 5- and 6-ring
824 compounds (> 80%). Measured PAH concentrations were significantly higher during

Deleted: The more specific outcomes of SAFIRED are outlined below.

Formatted: Font color: Text 1

Formatted: Font color: Text 1

Formatted: Font color: Text 1

Formatted: Heading 2

827 BBP2 and BBP4. During these periods, concentrations of BaP exceeded the monitoring
828 investigation level for atmospheric BaP (0.30 ng m^{-3}) in Australia (National-
829 Environment-Protection-Council-Service-Corporation, 2011) by up to 200%.
830
831 Biomass burning produces significant amounts of semi-volatile NMOC which can be
832 difficult to quantify and identify with current measurement techniques. However recent
833 studies have shown that including semi volatile NMOC chemistry in models improves
834 the agreement between the modeled and observed organic aerosol (Alvarado et al.,
835 2015; Konovalov et al., 2015) and ozone (Alvarado et al., 2015). High quality NMOC
836 emission factors are crucial for models to assess the impact of biomass burning plumes
837 on air quality and climate. Future analyses will be undertaken on the SAFIRED data to
838 quantify emission factors for various NMOCs.
839
840 SAFIRED represents the first measurements of atmospheric mercury undertaken in the
841 tropical region of the Australian continent. The mean observed GEM concentration
842 over the study period was 0.99 ± 0.09 ng m^{-3}, similar to the average over that month
843 (0.96 ng m^{-3}) for 5 other Southern Hemisphere sites and slightly lower than the average
844 (1.15 ng m^{-3}) for 5 tropical sites (Sprovieri et al., 2016). Mean GOM and PBM
845 concentrations were 11 ± 5 pg m^{-3} and 6 ± 3 pg m^{-3} respectively, representing 0.6 –
846 3.4% of total observed atmospheric mercury. During periods of pronounced trace gas
847 and aerosol concentrations during the campaign, spikes in GEM concentrations were
848 also observed, though there were no significant increases in GOM or PBM. Emission
849 ratios calculated during the campaign were two orders of magnitude higher than those
850 reported by Andreae and Merlet (2001). Future outcomes from the SAFIRED campaign
851 will focus on the use of micrometeorological techniques and the passive tracer radon to

quantify delivery of atmospheric mercury to tropical savannah ecosystems. ATARS also now serves as an additional site measuring continuous GEM as part of the Global Mercury Observation System (GMOS), one of only two tropical observing sites in the Eastern Hemisphere and the third such site located in Australia. A discussion of the seasonal and diurnal variations of atmospheric mercury at the ATARS site can be found in Howard et al. (2017).

4.2. Biomass burning aerosol chemistry

Milic et al., (2017) provided further analysis into the aerosol chemical composition to elucidate the aging of early dry season biomass burning emissions. Fractional analysis (e.g., f44 and f60, the fraction of m/z 44 and m/z 60 to all organic masses, indicated oxygenation and BB sources, respectively) and factor analysis using positive matrix factorisation (PMF) of cToF-AMS data was investigated over the entire sampling period. Outside of the periods of significant influence from BB events, three PMF-resolved organic aerosol factors were identified. A BB organic aerosol factor was found to comprise 24% of the submicron non-refractory organic mass, with an oxygenated organic aerosol factor and a biogenic isoprene-related secondary organic aerosol factor comprising 47% and 29%, respectively. These results indicate the significant influence of fresh and aged BB on aerosol composition in the early dry season. The emission of precursors from fires is likely responsible for some of the SOA formation.

The water uptake of aerosols during SAFIRED was further investigated in Mallet et al., (2017) to identify the influence of early dry season BB in this region on cloud formation. The concentrations of cloud condensation nuclei at a constant supersaturation of 0.5% were typically of the order of 2000 cm^{-3} and reached well over 10000 cm^{-3} during intense BB events. Variations in the ratio of aerosol particles

Deleted: Australian fires are responsible for 6% of ... [54]
Formatted ... [55]
Formatted ... [56]
Formatted ... [57]
Formatted ... [58]
Formatted ... [59]
Formatted ... [60]
Formatted ... [61]
Deleted: The gaseous and aerosol data for the sam ... [62]
Formatted ... [63]
Formatted ... [64]
Formatted ... [65]
Formatted ... [66]
Formatted ... [67]
Formatted ... [68]
Formatted ... [69]
Formatted ... [70]
Formatted ... [71]
Formatted ... [72]
Formatted ... [73]
Formatted ... [74]
Formatted ... [75]
Formatted ... [76]
Formatted ... [77]
Formatted ... [78]
Formatted ... [79]
Formatted ... [80]
Formatted ... [81]
Formatted ... [82]
Formatted ... [83]
Formatted ... [84]
Formatted ... [85]
Formatted ... [86]
Formatted ... [87]
Formatted ... [88]
Formatted ... [89]
Formatted ... [90]
Formatted ... [91]
Formatted ... [92]
Formatted ... [93]
Formatted ... [94]
Formatted ... [95]
Formatted ... [96]
Formatted ... [97]
Formatted ... [98]
Formatted ... [99]
Formatted ... [100]
Formatted ... [101]
Formatted ... [102]

activating cloud droplets showed a distinct diurnal trend, with an activation ratio of 40% ± 20% during the night and 60% ± 20% during the day. The particle size distribution and the hygroscopicity of the particles were found to significantly influence this activation ratio. Particles were generally extremely hydrophobic, particularly during the night and during the BB periods shown in this paper. Modelling CCN concentrations using the size distributions of aerosols and typical continental and terrestrial values of hygroscopicities yielded significant over predictions of up more than 200%, highlighting the need to include more regional parameterisations of aerosol composition and hygroscopicity.

Furthermore the fractional solubility of aerosol iron and other trace metals during SAFIRED were investigated in Winton et al., (2016). The fractional iron solubility is an important variable determining iron availability for biological uptake in the ocean. On a global scale, the large variability in the observed fractional iron solubility results, in part, from a mixture of different aerosol sources. Estimates of fractional iron solubility from fire combustion (1 - 60 %) are thought to be greater than those originating from mineral dust (1 - 2%) (Chuang et al., 2005;Guieu et al., 2005;Sedwick et al., 2007), and may vary in relationship to biomass and fire characteristics as well as that of the underlying terrain (Paris et al., 2010;Ito, 2011). Iron associated with BB may provide information with respect to BB inputs of iron to the ocean (Giglio et al., 2013;e.g. Meyer et al., 2008). The ATARS provides an ideal location to further investigate BB derived fractional iron solubility at the source. The results from this study can be found in Winton et al. (2016) and show that soluble iron concentrations from BB sources are significantly higher than those observed in Southern Ocean baseline air masses from the Cape Grim Baseline Air Pollution Station, Tasmania,

Formatted: Normal

Australia (Winton et al., 2015). Aerosol iron at SAFIRED was a mixture of fresh BB, mineral dust, sea spray and industrial pollution sources. The fractional iron solubility (2 - 12%) was relatively high throughout the campaign and the variability was related to the mixing and enhancement of mineral dust iron solubility with BB species.

5. Conclusions and looking forward

Biomass burning was found to significantly influence the surface atmospheric composition during the 2014 early dry season in north Australia. Over 28000 fires were detected via satellite retrieval during the sampling period. Several periods were identified when fires within 20 km of the research station resulted in significant enhancements of greenhouse gases, non-methane gaseous organic compounds, gaseous elemental mercury and polycyclic aromatic hydrocarbons and aerosol loadings. Much of the PM_1 mass was comprised of organic material. The aerosol particle number size distributions were typically unimodal and centered around 100 nm which is smaller than BBA observed in other regions. The analysis of the time series of these measured quantities has so far allowed the quantification of savannah fire emission factors for these aerosol and gaseous species and has provided and understanding of the aerosol aging, water uptake and solubility in this region.

While the specific outcomes of the SAFIRED campaign are reviewed in the previous section, the general importance of this study can be discussed in a greater context. This is the first large-scale collaborative project undertaken in this region and draws on the resources and expertise of most of Australia's research institutes focused on atmosphere chemistry and composition. Large scale, multidisciplinary measurement campaigns in the tropics, such as SAFIRED, are needed to make distinctions between different types

Formatted: Font color: Text 1

Comment [MM56]: R3:
16. While I understand that the majority of the companion papers that deal with the specifics of each measurement are in the process of being prepared or are currently under review, are there any novel campaign-wide conclusions that the authors would like to discuss in the concluding section of the manuscript?

Comment [MM57]: R3:
15. Clarification question: Were aircrafts used to study the biomass burning plumes?

Deleted: Atmospheric chemistry and radiative forcing will depend on how gaseous and aerosol emissions from fires age as they move and interact with each other and existing species in the atmosphere. Biomass burning aerosols can be involved in condensation and coagulation (Radhi et al., 2012), undergo water uptake (Mochida and Kawamura, 2004) form cloud droplets (Novakov and Corrigan, 1996), and be exposed to photochemical aging processes, including those involving the gaseous components of fire emissions (Keywood et al., 2011;Keywood et al., 2015). With a reported lifetime of 3.8 ± 0.8 days (Edwards et al., 2006), biomass burning aerosols are able to travel intercontinental distances (Rosen et al., 2000) and are therefore present in the atmosphere long enough for substantial changes due to aging. Furthermore, tropical convection is likely to affect the aging of BB emissions in the region around ATARS, due to the immediate proximity to the warm waters in the Timor Sea (Allen et al., 2008). This introduces further uncertainty to the effect of BB emissions on radiation flux. ... [103]

Deleted: L

Formatted: Font color: Text 1

Formatted: Font color: Text 1

Formatted: Font color: Text 1

Formatted: Font color: Text 1

Deleted: above

Formatted: Font color: Text 1

of fires in different regions to reduce uncertainties in global climate models (Keywood et al., 2013). This need has been recognized with the formation of global collaborative initiatives promoting interdisciplinary collaboration in biomass burning research (Kaiser and Keywood, 2015). As the world moves towards a warmer climate, it is plausible that the frequency and intensity of biomass burning will increase, and these emissions will become an increasingly important source of trace gases and aerosols to the atmosphere.

SAFIRED lays the foundation for future measurements at ATARS that could make measurements throughout the whole dry season and on a more long-term scale. Future work in this region should focus on 1) the detailed characterisation of individual fires and their emissions, 2) biomass burning emissions throughout the late dry season and 3) the vertical and horizontal transport of biomass burning emissions in this region. With well-established emission factors, a concentrated effort should be made to link modelled aerosol gaseous and aerosol loadings with *in situ* and remote sensing measurements. This should be done not just at the surface, but throughout the boundary layer as well as over the waters north of Australia. Furthermore, a further investigation of the radiative influence of the gaseous and aerosol species should be done for this region.

Data availability

All data are available upon request from the corresponding authors (Branka Miljevic, b.miljevic@qut.edu.au; Melita D. Keywood; melita.keywood@csiro.au).

Deleted: biomass burning is likely to increase in
Formatted: Font color: Text 1
Formatted: Font color: Text 1
Formatted: Font color: Text 1
Formatted: Font color: Text 1

Author Contributions

M.D. Mallet[a,b,c,d,e], M.J. Desservettaz[b,c,d,e], B. Miljevic[b,c,e*], A. Milic[b,d,e], Z.D. Ristovski[b,e], J. Alroe[b,c,e], L.T. Cravigan[b,c,e], E.R. Jayaratne[d,e], C. Paton-Walsh[b,c,e], D.W.T. Griffith[b,d,e], S.R. Wilson[b,d,e], G. Kettlewell[b,e], M.V. van der Schoot[b,e], P. Selleck[b,c,d,e], F. Reisen[b,c,e], S.J. Lawson[b,c,d,e], J. Ward[b,c,d,e], J. Harnwell[b,c,e], M. Cheng[b,c,d,e], R.W. Gillett[b,c,d,e], S.B. Molloy[d,e], D. Howard[b,c,d,e], P.F. Nelson[b,e], A.L Morrison[b,e], G.C. Edwards[b,c,e], A.G. Williams[b,c,e], S.D. Chambers[b,c,d,e], S. Werczynski[b,c,e], L.R. Williams[c,d,e], V.H.L. Winton[b,c,d,e], and B. Atkinson[b,c], X. Wang[b,d,e], M.D. Keywood[b,c,d,e,f*]

a: Wrote and organised the manuscript

b: Contributed to the organisation of the campaign

c: Installed and/or operated instrumentation during the sampling period

d: Analysed data

e: Contributed to the manuscript and/or data interpretation

f: Designed and led the campaign.

*: Corresponding author

Competing interests

The authors declare that they have no conflict of interest.

Acknowledgements

The majority of the campaign was internally funded. The input of QUT was supported by the Australian Research Council Discovery (Grant DP120100126). The work on aerosol iron solubility was supported by Curtin University (RES-SE-DAP_AW-47679-

1), the University of Tasmania (B0019024) and the Australian Research Council (Grant FT130100037).

6. References

Akagi, S. K., Craven, J. S., Taylor, J. W., McMeeking, G. R., Yokelson, R. J., Burling, I. R., Urbanski, S. P., Wold, C. E., Seinfeld, J. H., Coe, H., Alvarado, M. J., and Weise, D. R.: Evolution of trace gases and particles emitted by a chaparral fire in California, Atmospheric Chemistry and Physics, 12, 1397-1421, 2012.

Andersen, A. N., Cook, G. D., Corbett, L. K., Douglas, M. M., Eager, R. W., Russell-Smith, J., Setterfield, S. A., Williams, R. J., and Woinarski, J. C.: Fire frequency and biodiversity conservation in Australian tropical savannas: implications from the Kapalga fire experiment, Austral Ecology, 30, 155-167, 2005.

Bindoff, N. L., Stott, P. A., AchutaRao, K. M., Allen, M. R., Gillett, N., Gutzler, D., Hansingo, K., Hegerl, G., Hu, Y., Jain, S., Mokhov, I. I., Overland, J., Perlwitz, J., Sebbari, R., and Zhang, X.: Detection and Attribution of Climate Change: from Global to Regional, in: Climate Change 2013: The Physical Science Basis. Contribution of Working Group I to the Fifth Assessment Report of the Intergovernmental Panel on Climate Change, edited by: Stocker, T. F., Qin, D., Plattner, G.-K., Tignor, M., Allen, S. K., Boschung, J., Nauels, A., Xia, Y., Bex, V., and Midgley, P. M., Cambridge University Press, Cambridge, United Kingdom and New York, NY, USA, 867–952, 2013.

Chambers, S. D., Hong, S.-B., Williams, A. G., Crawford, J., Griffiths, A. D., and Park, S.-J.: Characterising terrestrial influences on Antarctic air masses using Radon-222 measurements at King George Island, Atmospheric Chemistry and Physics, 14, 9903-9916, 2014.

Chow, J. C., Watson, J. G., Chen, L. W. A., Chang, M. C. O., Robinson, N. F., Trimble, D., and Kohl, S.: The IMPROVE-A temperature protocol for thermal/optical carbon analysis: maintaining consistency with a long-term database, Journal of the Air & Waste Management Association, 57, 1014-1023, 2007a.

Chow, J. C., Watson, J. G., Chen, L. W. A., Chang, M. O., Robinson, N. F., Trimble, D., and Kohl, S.: The IMPROVE-A temperature protocol for thermal/optical carbon analysis: maintaining consistency with a long-term database, Journal of the Air & Waste Management Association, 57, 1014-1023, 2007b.

Chuang, P. Y., Duvall, R. M., Shafer, M. M., and Schauer, J. J.: The origin of water soluble particulate iron in the Asian atmospheric outflow, Geophysical Research Letters, 32, L07813, 2005.

Crutzen, P. J., and Andreae, M. O.: Biomass burning in the tropics: Impact on atmospheric chemistry and biogeochemical cycles, Science, 250, 1669-1678, 1990.

Desservettaz, M., Paton-Walsh, C., Griffith, D. W., Kettlewell, G., Keywood, M. D., Vanderschoot, M. V., Ward, J., Mallet, M. D., Milic, A., and Miljevic, B.: Emission factors of trace gases and particles from tropical savanna fires in Australia, Journal of Geophysical Research: Atmospheres, 2017.

Draxler, R. R., and Rolph, G.: HYSPLIT (HYbrid Single-Particle Lagrangian Integrated Trajectory) model access via NOAA ARL READY website (http://www/.

Formatted: Font color: Text 1, Spanish

arl. noaa. gov/ready/hysplit4. html). NOAA Air Resources Laboratory, Silver Spring, in, Md, 2003.
Du, H., Kong, L., Cheng, T., Chen, J., Du, J., Li, L., Xia, X., Leng, C., and Huang, G.: Insights into summertime haze pollution events over Shanghai based on online water-soluble ionic composition of aerosols, Atmospheric Environment, 45, 5131-5137, 2011.
Dunne, E., Galbally, I. E., Cheng, M., Selleck, P., Molloy, S. B., and Lawson, S. J.: Comparison of VOC measurements made by PTR-MS, Adsorbent Tube/GC-FID-MS and DNPH-derivatization/HPLC during the Sydney Particle Study, 2012: a contribution to the assessment of uncertainty in current atmospheric VOC measurements, Atmos. Meas. Tech. Discuss, 2017, 1-24, 2017.
Edwards, G. C., Rasmussen, P. E., Schroeder, W. H., Wallace, D. M., Halfpenny-Mitchell, L., Dias, G. M., Kemp, R. J., and Ausma, S.: Development and evaluation of a sampling system to determine gaseous Mercury fluxes using an aerodynamic micrometeorological gradient method, Journal of Geophysical Research: Atmospheres, 110, 2005.
Ferek, R. J., Reid, J. S., Hobbs, P. V., Blake, D. R., and Liousse, C.: Emission factors of hydrocarbons, halocarbons, trace gases and particles from biomass burning in Brazil, Journal of Geophysical Research, 103, 107-132, 1998.
Giglio, L., Randerson, J. T., and Werf, G. R.: Analysis of daily, monthly, and annual burned area using the fourth-generation global fire emissions database (GFED4), Journal of Geophysical Research: Biogeosciences, 118, 317-328, 2013.
Govender, N., Trollope, W. S., and Van Wilgen, B. W.: The effect of fire season, fire frequency, rainfall and management on fire intensity in savanna vegetation in South Africa, Journal of Applied Ecology, 43, 748-758, 2006.
Griffith, D. W. T.: Synthetic calibration and quantitative analysis of gas-phase FT-IR spectra, Applied Spectroscopy, 50, 59-70, 1996.
Griffith, D. W. T., Deutscher, N. M., Caldow, C., Kettlewell, G., Riggenbach, M., and Hammer, S.: A Fourier transform infrared trace gas and isotope analyser for atmospheric applications, Atmos. Meas. Tech., 5, 2481-2498, 2012.
Guieu, C., Bonnet, S., Wagener, T., and Loÿe-Pilot, M. D.: Biomass burning as a source of dissolved iron to the open ocean?, Geophysical Research Letters, 32, 2005.
Gustin, M. S., Lindberg, S. E., and Weisberg, P. J.: An update on the natural sources and sinks of atmospheric mercury, Applied Geochemistry, 23, 482-493, 2008.
Honninger, G., von Friedeburg, C., and Platt, U.: Multi axis differential optical absorption spectroscopy (MAX-DOAS), Atmospheric Chemistry and Physics, 4, 231-254, 2004.
Howard, D., Nelson, P. F., Edwards, G. C., Morrison, A. L., Fisher, J. A., Ward, J., Harnwell, J., van der Schoot, M., Atkinson, B., Chambers, S. D., Griffiths, A. D., Werczynski, S., and Williams, A. G.: Atmospheric mercury in the southern hemisphere tropics: seasonal and diurnal variations and influence of inter-hemispheric transport, Atmos. Chem. Phys. Discuss., 2017, 1-20, 10.5194/acp-2017-307, 2017.
Iinuma, Y., Engling, G., Puxbaum, H., and Herrmann, H.: A highly resolved anion-exchange chromatographic method for determination of saccharidic tracers for biomass combustion and primary bio-particles in atmospheric aerosol, Atmospheric Environment, 43, 1367-1371, 2009.
Ito, A.: Mega fire emissions in Siberia: potential supply of bioavailable iron from forests to the ocean, Biogeosciences, 8, 1679-1697, 2011.
Jacobson, M. Z.: Strong radiative heating due to the mixing state of black carbon in atmospheric aerosols, Nature, 409, 695-697, 2001.

1120 Kaiser, J. W., and Keywood, M.: Preface for Atmos. Env. Special issue on IBBI,
1121 Atmospheric Environment, 121, 1-3, 2015.
1122 Keil, A., and Haywood, J. M.: Solar radiative forcing by biomass burning aerosol
1123 particles during SAFARI 2000: A case study based on measured aerosol and cloud
1124 properties, Journal of Geophysical Research: Atmospheres, 108, 2003.
1125 Keywood, M., Kanakidou, M., Stohl, A., Dentener, F., Grassi, G., Meyer, C. P.,
1126 Torseth, K., Edwards, D., Thompson, A. M., Lohmann, U., and Burrows, J.: Fire in the
1127 air: Biomass burning impacts in a changing climate, Critical Reviews in Environmental
1128 Science and Technology, 43, 40-83, 2013.
1129 Landis, M. S., Stevens, R. K., Schaedlich, F., and Prestbo, E. M.: Development and
1130 characterization of an annular denuder methodology for the measurement of divalent
1131 inorganic reactive gaseous mercury in ambient air, Environmental science &
1132 technology, 36, 3000-3009, 2002.
1133 LaRoche, J., and Breitbarth, E.: Importance of the diazotrophs as a source of new
1134 nitrogen in the ocean, Journal of Sea Research, 53, 67-91, 2005.
1135 Lawson, S. J., Keywood, M. D., Galbally, I. E., Gras, J. L., Cainey, J. M., Cope, M. E.,
1136 Krummel, P. B., Fraser, P. J., Steele, L. P., Bentley, S. T., Meyer, C. P., Ristovski, Z.,
1137 and Goldstein, A. H.: Biomass burning emissions of trace gases and particles in marine
1138 air at Cape Grim, Tasmania, Atmospheric Chemistry and Physics, 15, 13393-13411,
1139 2015.
1140 Lin, N.-H., Tsay, S.-C., Maring, H. B., Yen, M.-C., Sheu, G.-R., Wang, S.-H., Chi, K.
1141 H., Chuang, M.-T., Ou-Yang, C.-F., and Fu, J. S.: An overview of regional experiments
1142 on biomass burning aerosols and related pollutants in Southeast Asia: From BASE-
1143 ASIA and the Dongsha Experiment to 7-SEAS, Atmospheric Environment, 78, 1-19,
1144 2013.
1145 Liousse, C., Devaux, C., Dulac, F., and Cachier, H.: Aging of savanna biomass burning
1146 aerosols: Consequences on their optical properties, Journal of Atmospheric Chemistry,
1147 22, 1-17, 1995.
1148 Manninen, H. E., Petaja, T., Asmi, E., Riipinen, I., Nieminen, T., Mikkila, J., Horrak,
1149 U., Mirme, A., Mirme, S., Laakso, L., Kerminen, V. M., and Kulmala, M.: Long-term
1150 field measurements of charged and neutral clusters using Neutral cluster and Air Ion
1151 Spectrometer (NAIS), Boreal Environment Research, 14, 591-605, 2009.
1152 Meyer, C., Cook, G., Reisen, F., Smith, T., Tattaris, M., Russell-Smith, J., Maier, S.,
1153 Yates, C., and Wooster, M.: Direct measurements of the seasonality of emission factors
1154 from savanna fires in northern Australia, Journal of Geophysical Research:
1155 Atmospheres (1984–2012), 117, 2012.
1156 Meyer, C. P., Luhar, A. K., and Mitchell, R. M.: Biomass burning emissions over
1157 northern Australia constrained by aerosol measurements: I—Modelling the distribution
1158 of hourly emissions, Atmospheric Environment, 42, 1629-1646, 2008.
1159 Mirme, A., Tamm, E., Mordas, G., Vana, M., Uin, J., Mirme, S., Bernotas, T., Laakso,
1160 L., Hirsikko, A., and Kulmala, M.: A wide-range multi-channel Air Ion Spectrometer,
1161 Boreal Environmental Research, 12, 247-264, 2007.
1162 National-Environment-Protection-Council-Service-Corporation: National
1163 Environment Protection (Air Toxics) Measure, 2011.
1164 Paris, R., Desboeufs, K., Formenti, P., Nava, S., and Chou, C.: Chemical
1165 characterisation of iron in dust and biomass burning aerosols during AMMA-
1166 SOP0/DABEX: implication for iron solubility, Atmospheric Chemistry and Physics,
1167 10, 4273-4282, 2010.
1168 Penner, J., Chuang, C., and Grant, K.: Climate forcing by carbonaceous and sulfate
1169 aerosols, Climate Dynamics, 14, 839-851, 1998.

1170 Rea, A. W., Lindberg, S. E., Scherbatskoy, T., and Keeler, G. J.: Mercury accumulation
1171 in foliage over time in two northern mixed-hardwood forests, Water, Air, and Soil
1172 Pollution, 133(1-4), 49-67, 2002.
1173 Russell-Smith, J., Yates, C. P., Whitehead, P. J., Smith, R., Craig, R., Allan, G. E.,
1174 Thackway, R., Frakes, I., Cridland, S., Meyer, M. C. P., and Gill, M.: Bushfires' down
1175 under': patterns and implications of contemporary Australian landscape burning,
1176 International Journal of Wildland Fire, 16, 361-377, 2007.
1177 Russell-Smith, J., Cook, G. D., Cooke, P. M., Edwards, A. C., Lendrum, M., Meyer,
1178 C., and Whitehead, P. J.: Managing fire regimes in north Australian savannas: applying
1179 Aboriginal approaches to contemporary global problems, Frontiers in Ecology and the
1180 Environment, 11, e55-e63, 2013.
1181 Saarikoski, S., Sillanpää, M., Sofiev, M., Timonen, H., Saarnio, K., Teinilä, K.,
1182 Karppinen, A., Kukkonen, J., and Hillamo, R.: Chemical composition of aerosols
1183 during a major biomass burning episode over northern Europe in spring 2006:
1184 Experimental and modelling assessments, Atmospheric Environment, 41, 3577-3589,
1185 2007.
1186 Sedwick, P. N., Sholkovitz, E. R., and Church, T. M.: Impact of anthropogenic
1187 combustion emissions on the fractional solubility of aerosol iron: Evidence from the
1188 Sargasso Sea, Geochemistry, Geophysics, Geosystems, 8, 2007.
1189 Shi, Y., Matsunaga, T., Saito, M., Yamaguchi, Y., and Chen, X.: Comparison of global
1190 inventories of CO_2 emissions from biomass burning during 2002–2011 derived from
1191 multiple satellite products, Environmental Pollution, 206, 479-487, 2015.
1192 Singh, H., Brune, W., Crawford, J., Jacob, D. J., and Russell, P.: Overview of the
1193 summer 2004 Intercontinental Chemical Transport Experiment–North America
1194 (INTEX-A), Journal of Geophysical Research: Atmospheres, 111, 2006.
1195 Sinreich, R., Friess, U., Wagner, T., and Platt, U.: Multi axis differential optical
1196 absorption spectroscopy (MAX-DOAS) of gas and aerosol distributions, Faraday
1197 Discuss, 130, 153-164, 2005.
1198 Sprovieri, F., Pirrone, N., Bencardino, M., D'Amore, F., Carbone, F., Cinnirella, S.,
1199 Mannarino, V., Landis, M., Ebinghaus, R., Weigelt, A., Brunke, E. G., Labuschagne,
1200 C., Martin, L., Munthe, J., Wängberg, I., Artaxo, P., Morais, F., Cairns, W., Barbante,
1201 C., Diéguez, M. D. C., Garcia, P. E., Dommergue, A., Angot, H., Magand, O., Skov,
1202 H., Horvat, M., Kotnik, J., Read, K. A., Neves, L. M., Gawlik, B. M., Sena, F.,
1203 Mashyanov, N., Obolkin, V. A., Wip, D., Feng, X. B., Zhang, H., Fu, X.,
1204 Ramachandran, R., Cossa, D., Knoery, J., Marusczak, N., Nerentorp, M., and Norstrom,
1205 C.: Atmospheric Mercury Concentrations observed at ground-based monitoring sites
1206 globally distributed in the framework of the GMOS network, Atmospheric Chemistry
1207 and Physics Discussions, 2016, 1-32, 2016.
1208 Steffen, A., Douglas, T., Amyot, M., Ariya, P., Aspmo, K., Berg, T., Bottenheim, J.,
1209 Brooks, S., Cobbett, F., Dastoor, A., Dommergue, A., Ebinghaus, R., Ferrari, C.,
1210 Gardfeldt, K., Goodsite, M. E., Lean, D., Poulain, A. J., Scherz, C., Skov, H., Sommar,
1211 J., and Temme, C.: A synthesis of atmospheric mercury depletion event chemistry in
1212 the atmosphere and snow, Atmospheric Chemistry and Physics, 8, 1445-1482, 2008.
1213 Stockwell, C., Yokelson, R., Kreidenweis, S., Robinson, A., DeMott, P., Sullivan, R.,
1214 Reardon, J., Ryan, K., Griffith, D., and Stevens, L.: Trace gas emissions from
1215 combustion of peat, crop residue, domestic biofuels, grasses, and other fuels:
1216 configuration and Fourier transform infrared (FTIR) component of the fourth Fire Lab
1217 at Missoula Experiment (FLAME-4), Atmospheric Chemistry and Physics, 9727, 2014.

Tuch, T. M., Haudek, A., Müller, T., Nowak, A., Wex, H., and Wiedensohler, A.: Design and performance of an automatic regenerating adsorption aerosol dryer for continuous operation at monitoring sites, Atmos. Meas. Tech., 2, 417-422, 2009.

van der Werf, G. R., Randerson, J. T., Giglio, L., Collatz, G., Mu, M., Kasibhatla, P. S., Morton, D. C., DeFries, R., Jin, Y. v., and van Leeuwen, T. T.: Global fire emissions and the contribution of deforestation, savanna, forest, agricultural, and peat fires (1997–2009), Atmospheric Chemistry and Physics, 10, 11707-11735, 2010.

Wang, X., Thai, P. K., Mallet, M., Desservettaz, M., Hawker, D. W., Keywood, M., Miljevic, B., Paton-Walsh, C., Gallen, M., and Mueller, J. F.: Emissions of selected semivolatile organic chemicals from forest and savannah fires, Environmental science & technology, 51, 1293-1302, 2017.

Whittlestone, S., and Zahorowski, W.: Baseline radon detectors for shipboard use: Development and deployment in the First Aerosol Characterization Experiment (ACE 1), Journal of Geophysical Research: Atmospheres, 103, 16743-16751, 1998.

Winton, V., Bowie, A., Edwards, R., Keywood, M., Townsend, A., van der Merwe, P., and Bollhöfer, A.: Fractional iron solubility of atmospheric iron inputs to the Southern Ocean, Marine Chemistry, 177, 20-32, 2015.

Winton, V., Edwards, R., Bowie, A., Keywood, M., Williams, A., Chambers, S., Selleck, P., Desservettaz, M., Mallet, M., and Paton-Walsh, C.: Dry season aerosol iron solubility in tropical northern Australia, Atmospheric Chemistry and Physics Discussions, doi:10.5194/acp-2016-419, 2016.

Wong, J., and Li, Z.: Retrieval of optical depth for heavy smoke aerosol plumes: uncertainties and sensitivities to the optical properties, Journal of the Atmospheric Sciences, 59, 250-261, 2002.

Yokelson, R. J., Crounse, J. D., DeCarlo, P. F., Karl, T., Urbanski, S., Atlas, E., Campos, T., Shinozuka, Y., Kapustin, V., Clarke, A. D., Weinheimer, A., Knapp, D. J., Montzka, D. D., Holloway, J., Weibring, P., Flocke, F., Zheng, W., Toohey, D., Wennberg, P. O., Wiedinmyer, C., Mauldin, L., Fried, A., Richter, D., Walega, J., Jimenez, J. L., Adachi, K., Buseck, P. R., Hall, S. R., and Shetter, R.: Emissions from biomass burning in the Yucatan, Atmospheric Chemistry and Physics, 9, 5785-5812, 2009.

Formatted: Justified, Line spacing: double

Formatted: Font color: Text 1

Formatted: Heading 1

1251

Page 10: [1] Formatted	Marc Mallet	3/27/17 1:37:00 AM

Caption, Keep with next

Page 10: [2] Formatted	Marc Mallet	3/27/17 1:35:00 AM

Left: 1", Right: 1", Top: 1.25", Bottom: 1.25", Width: 11.69", Height: 8.26", Header distance from edge: 0.49", Footer distance from edge: 0.49"

Page 10: [3] Formatted Table	Marc Mallet	9/15/17 7:54:00 AM

Formatted Table

Page 10: [4] Formatted	Marc Mallet	9/14/17 9:29:00 PM

Subscript

Page 10: [4] Formatted	Marc Mallet	9/14/17 9:29:00 PM

Subscript

Page 10: [4] Formatted	Marc Mallet	9/14/17 9:29:00 PM

Subscript

Page 10: [4] Formatted	Marc Mallet	9/14/17 9:29:00 PM

Subscript

Page 10: [4] Formatted	Marc Mallet	9/14/17 9:29:00 PM

Subscript

Page 10: [4] Formatted	Marc Mallet	9/14/17 9:29:00 PM

Subscript

Page 10: [4] Formatted	Marc Mallet	9/14/17 9:29:00 PM

Subscript

Page 10: [4] Formatted	Marc Mallet	9/14/17 9:29:00 PM

Subscript

Page 10: [4] Formatted	Marc Mallet	9/14/17 9:29:00 PM

Subscript

Page 10: [5] Formatted **Marc Mallet** **9/14/17 9:09:00 PM**

Subscript

Page 10: [5] Formatted **Marc Mallet** **9/14/17 9:09:00 PM**

Subscript

Page 10: [5] Formatted **Marc Mallet** **9/14/17 9:09:00 PM**

Subscript

Page 10: [5] Formatted **Marc Mallet** **9/14/17 9:09:00 PM**

Subscript

Page 10: [6] Formatted **Marc Mallet** **9/14/17 4:34:00 PM**

Font:8 pt

Page 10: [6] Formatted **Marc Mallet** **9/14/17 4:34:00 PM**

Font:8 pt

Page 10: [7] Formatted **Marc Mallet** **5/15/17 12:51:00 AM**

Font:8 pt

Page 10: [7] Formatted **Marc Mallet** **5/15/17 12:51:00 AM**

Font:8 pt

Page 10: [8] Formatted **Marc Mallet** **5/15/17 12:51:00 AM**

Font:8 pt

Page 10: [9] Formatted **Marc Mallet** **9/11/17 9:52:00 AM**

Superscript

Page 10: [10] Formatted **Marc Mallet** **5/15/17 12:51:00 AM**

Font:8 pt

Page 10: [11] Formatted **Marc Mallet** **9/11/17 9:13:00 AM**

Superscript

Page 10: [11] Formatted **Marc Mallet** **9/11/17 9:13:00 AM**

Superscript

Page 10: [11] Formatted **Marc Mallet** **9/11/17 9:13:00 AM**

Superscript

Page 10: [12] Formatted **Marc Mallet** **9/15/17 7:56:00 AM**

Font:Bold, Superscript

Page 10: [13] Formatted **Marc Mallet** **6/15/17 9:00:00 AM**

Font:Not Bold

Page 10: [14] Formatted **Marc Mallet** **6/15/17 9:00:00 AM**

Font:8 pt

Page 10: [15] Formatted **Marc Mallet** **5/15/17 12:52:00 AM**

Centered, Position:Horizontal: Left, Relative to: Column, Vertical: 0", Relative to: Paragraph, Horizontal: 0.13", Wrap Around

Page 10: [16] Formatted **Marc Mallet** **5/15/17 12:51:00 AM**

Font:8 pt

Page 10: [17] Formatted **Marc Mallet** **5/15/17 12:52:00 AM**

Centered, Position:Horizontal: Left, Relative to: Column, Vertical: 0", Relative to: Paragraph, Horizontal: 0.13", Wrap Around

Page 10: [18] Formatted **Marc Mallet** **5/15/17 12:51:00 AM**

Font:8 pt

Page 10: [19] Formatted **Marc Mallet** **5/15/17 12:52:00 AM**

Centered, Position:Horizontal: Left, Relative to: Column, Vertical: 0", Relative to: Paragraph, Horizontal: 0.13", Wrap Around

Page 10: [20] Formatted **Marc Mallet** **5/15/17 12:51:00 AM**

Font:8 pt

Page 10: [21] Formatted **Marc Mallet** **9/11/17 9:16:00 AM**

Subscript

Page 10: [21] Formatted **Marc Mallet** **9/11/17 9:16:00 AM**

Subscript

Page 10: [22] Formatted **Marc Mallet** **5/15/17 12:52:00 AM**

Centered, Position:Horizontal: Left, Relative to: Column, Vertical: 0", Relative to: Paragraph, Horizontal: 0.13", Wrap Around

Page 10: [23] Formatted **Marc Mallet** **5/15/17 12:51:00 AM**

Font:8 pt

Page 10: [24] Formatted **Marc Mallet** **9/14/17 9:00:00 PM**

Superscript

Page 10: [25] Formatted **Marc Mallet** **9/11/17 9:16:00 AM**

Subscript

Page 10: [26] Formatted **Marc Mallet** **5/15/17 12:52:00 AM**

Centered, Position:Horizontal: Left, Relative to: Column, Vertical: 0", Relative to: Paragraph, Horizontal: 0.13", Wrap Around

Page 10: [27] Formatted **Marc Mallet** **5/15/17 12:51:00 AM**

Font:8 pt

Page 10: [28] Formatted **Marc Mallet** **9/15/17 7:53:00 AM**

Superscript

Page 10: [29] Formatted **Marc Mallet** **9/11/17 9:16:00 AM**

Subscript

Page 10: [30] Formatted **Marc Mallet** **5/15/17 12:51:00 AM**

Font:8 pt

Page 10: [31] Formatted **Marc Mallet** **5/15/17 12:52:00 AM**

Centered, Position:Horizontal: Left, Relative to: Column, Vertical: 0", Relative to: Paragraph, Horizontal: 0.13", Wrap Around

Page 10: [32] Formatted **Marc Mallet** **9/11/17 9:14:00 AM**

Superscript

Page 10: [32] Formatted **Marc Mallet** **9/11/17 9:14:00 AM**

Superscript

Page 10: [32] Formatted **Marc Mallet** **9/11/17 9:14:00 AM**

Superscript

Page 10: [32] Formatted **Marc Mallet** **9/11/17 9:14:00 AM**

Superscript

Page 10: [32] Formatted **Marc Mallet** **9/11/17 9:14:00 AM**

Superscript

Page 10: [32] Formatted **Marc Mallet** **9/11/17 9:14:00 AM**

Superscript

Page 10: [32] Formatted **Marc Mallet** **9/11/17 9:14:00 AM**

Superscript

Page 10: [32] Formatted **Marc Mallet** **9/11/17 9:14:00 AM**

Superscript

Page 10: [33] Formatted **Marc Mallet** **5/15/17 12:52:00 AM**

Centered, Position:Horizontal: Left, Relative to: Column, Vertical: 0", Relative to: Paragraph, Horizontal: 0.13", Wrap Around

Page 10: [34] Formatted **Marc Mallet** **5/15/17 12:51:00 AM**

Font:8 pt

Page 10: [35] Formatted	Marc Mallet	9/11/17 9:46:00 AM

Line spacing: double

Page 10: [36] Formatted	Marc Mallet	9/14/17 9:07:00 PM

Keep with next

Page 16: [37] Deleted	Marc Mallet	5/1/17 10:12:00 PM

Radon-222 (radon) is a naturally occurring radioactive noble gas that arises from the alpha-particle decay of radium-226, which is ubiquitous in most soil and rock types. With a half-life of 3.82 days, radon has thus proven to be an excellent indicator of recent (within 2-3 weeks) terrestrial influences on air masses for observations at coastal or island sites (Chambers et al., 2014). Radon is unreactive and poorly soluble, and its only atmospheric sink is radioactive decay. Furthermore, it has a half-life comparable to the lifetimes of short-lived atmospheric pollutants (e.g., NOx, SO_2) and atmospheric residence time of water and aerosols[MM1]. Radon's unique combination of physical characteristics make it an ideal tracer for (i) regional air mass transport studies, in which it is often used in conjunction with air mass back trajectories for fetch [MM2]analyses (Williams et al., 2009;Chambers et al., 2014); (ii) investigations of vertical mixing processes within the daytime convective boundary layer (Williams et al., 2011) or nocturnal boundary layer (Chambers et al., 2015); (iii) identifying periods of minimal terrestrial influence on a measured air mass ("baseline" studies; (Chambers et al., 2016)); (iv) performing regional flux or inventory analyses for trace atmospheric species with similar source distributions (Biraud et al., 2000) and (v) evaluating the performance of transport and mixing schemes in climate and chemical-transport models (Locatelli et al., 2015).

Page 26: [38] Deleted	Marc Mallet	5/2/17 1:32:00 AM

Afternoon radon concentrations provide further information regarding the regional air mass fetch and the degree of contact with the land surface (red line, Figure 3a). Over the campaign period, air masses with the least terrestrial fetch (low radon indicates strongest oceanic signature) were observed on June 4-6 and 20-22, whereas June 8-9, 17-18 and 29-30 represented periods of particularly extensive continental fetch.

Page 27: [39] Deleted	Marc Mallet	5/2/17 1:31:00 AM

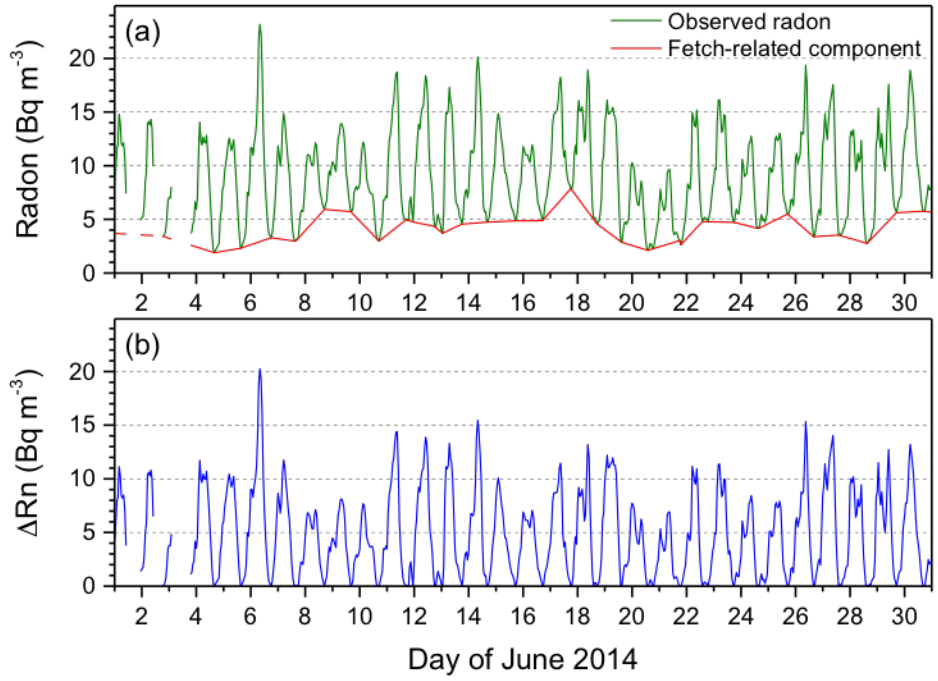

Figure **3** Hourly ATARS radon observations for June 2014: (a) observed hourly data, and afternoon-to-afternoon interpolated values (indicative of changes in the regional air mass fetch); and (b) difference in radon concentration between the hourly observations and interpolated afternoon values (indicative of diurnal variability).

A pronounced diurnal variability can clearly be seen in the ΔRn signal (Figure 3b). Mean hourly diurnal composites of radon concentrations, wind speed, wind direction and dew point temperature at the ATARS site during the period of the SAFIRED campaign are shown in Figure 4. Following the technique described in Chambers et al. (2016), these composites have been computed separately for three diurnal mixing categories based on the mean ΔRn over the 12 hour period 2000-0800 h:

Strong mixing: $\Delta Rn_{12} < 5400$ mBq m^{-3}

Moderate mixing: $5400 \leq \Delta Rn_{12} < 6700$ mBq m^{-3}

Weak mixing: $\Delta Rn_{12} \geq 6700$ mBq m^{-3}

The air masses predominantly originated from the southeast as indicated in Figure 1 and Figure 4c. Starting from approximately 10:00 am each morning, however, sea breeze circulations slowly turn the measured wind direction around from southeast to northeast, before reverting back to the dominant wind direction again at around midnight. Wind speeds reached a maximum just before midday and were at their lowest just before midnight (Figure 4b). The "strong mixing" category was associated with generally higher wind speeds, which cause increased mechanical turbulence leading to deeper nocturnal mixing layers (i.e., hinder the development of a shallow nocturnal inversion layer).[MM3]

Page 32: [40] Deleted **Marc Mallet** **5/14/17 10:38:00 PM**

Gas and Aerosol measurements

The campaign average, standard deviation, median and Q25/Q75 values for the major gaseous and aerosol species are shown in Table 1. The median values for each species are likely to be representative of background concentrations in this region[MM4]. The average concentrations for most species were higher than the median concentrations, due to the periods of close or intense fires. The extent of the influence of these close fires are demonstrated by the maximum concentrations.

Table **1** The campaign average, standard deviation, maximum, median, Q25 and Q75 values for key measured gas and aerosol species. All parts-per notation refer to mole fractions unless otherwise indicated.

Species (unit)	Average	Standard deviation	Maximum	Median	Q25	Q75
CO (ppb)	229	494	18900	130	87	214
CO_2 (ppm)	404.68	11.539	513.578	402.454	394.728	411.299
O_3 (ppbv)	24.616	9.903	99.784	22.771	17.896	29.778

CH_4 (ppb)	1839.88	68.06	3766.81	1820.11	1802.26	1852.97
N_2O (ppb)	326.329	0.449	334.871	326.276	326.121	326.444
GEM (ng m^{-3})	0.992	0.081	1.734	0.986	0.952	1.020
Acetonitrile (ppb)	0.351	0.629	9.775	0.197	0.129	0.337
Organics (ug m^{-3})	11.081	22.385	347.657	4.160	2.335	13.279
SO_4^{2-} (ug m^{-3})	0.514	0.318	2.254	0.411	0.294	0.679
NH_4^+ (ug m^{-3})	0.351	0.676	18.17	0.180	0.096	0.415
NO_3^- (ug m^{-3})	0.187	0.456	10.925	0.042	0.004	0.189
Cl^- (ug m^{-3})	0.166	1.271	53.270	0.029	0.016	0.076
PNC (cm^{-3})	8182	19031	40300	2032	2032	8335
Mode diameter (nm)	104	31	-	102	85	122
Geom. SD	1.71	0.13	-	1.70	1.65	1.75

[MM5][MM6]

In order to demonstrate the influence of close fires and the changing inversion layer, the time series of major greenhouse gases (CO, CO_2, CH_4 and N_2O), gaseous elemental mercury, acetonitrile and ozone throughout the campaign are shown in Figure 5. Sub-micron non-refractory aerosol organic, sulfate, ammonium and nitrate mass concentrations, organic mass fraction, PM_1 OC and EC mass concentrations and particle size distributions for the sampling period are shown in Figure 6. Periods of missing data correspond to times when instruments were not operating. Most of these time series display a clear diurnal trend as a result of the varying inversion layer height. Other enhancements in concentrations can be clearly seen and correspond to periods of frequent close

fires (Figure 2). [MM7]Over the entire sampling period from the 29th of May 2014 until the 28th of June 2014, four biomass burning related periods (BBP) and a "coastal" period (CP) have been distinguished. The dates for these periods are shown in Table 2. These periods are also displayed in Figure 5 and Figure 6. [MM8]

Table 2 The start and end dates for the four identified Biomass Burning Periods (BBP1, BBP2, BBP3 and BBP4) and the Coastal Period (CP).

Period	**Start date** **(mm/dd/yy hh:mm)**	**End date** **(mm/dd/yy hh:mm)**
BBP1	05/30/14 00:00	05/31/14 23:59
BBP2	06/06/14 00:00	06/12/14 23:59
BBP3	06/14/14 00:00	06/17/14 23:59
CP	06/19/14 12:00	06/22/14 23:59
BBP3	06/23/14 00:00	06/28/14 23:59

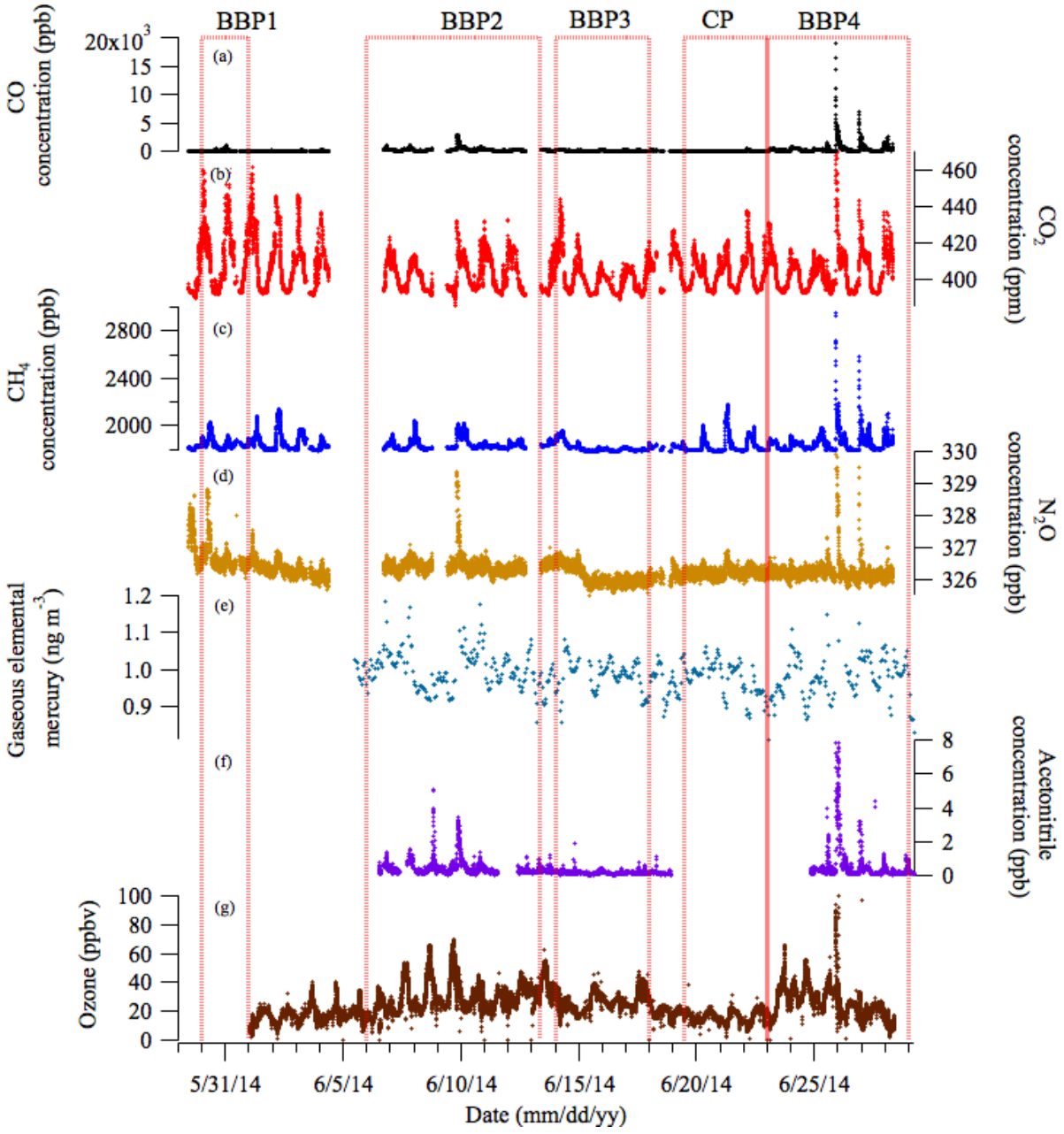

[MM9]

Figure **5** The time series of the major measured gaseous species during the SAFIRED campaign: (a) carbon monoxide, (b) carbon dioxide, (c) methane, (d) nitrogen dioxide[MM10], (e) gaseous elemental mercury, (f) acetonitrile and (g) ozone and $\Delta O_3/\Delta CO$. The biomass burning and coastal periods are indicated by the red dotted lines. All parts-per notation refer to mole fractions unless otherwise indicated.

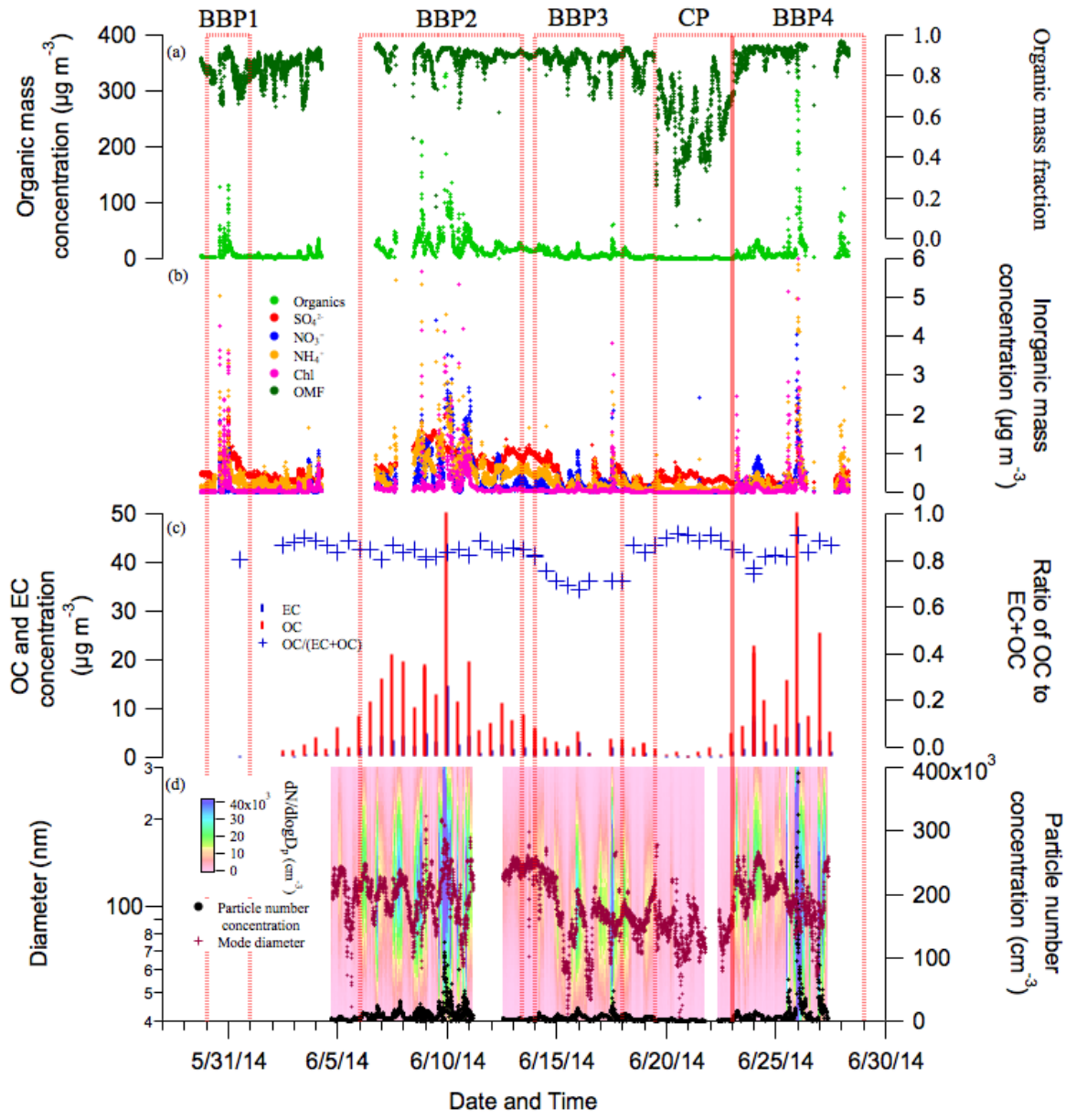

[MM11]

Figure **6** The times series of the major aerosol properties during the SAFIRED campaign: (a) the non-refractory PM_1 organic mass concentration (left) and organic mass fraction (right), b) the inorganic non-refractory PM_1 mass concentrations, (c) the 12-hour filter OC and EC PM_1 mass concentrations (left) and the ratio of OC to OC+EC (right), (d) the particle size distributions and particle size mode (left) and the total particle number concentration (right) and (e) the wind direction at ATARS.

Over the campaign organics dominated the non-refectory sub-micron aerosol mass contributing, on average 90% (median; 86%) of the total mass. Sulphate, nitrates, ammonium and chloride species contributed the rest of this mass, with the largest contributions from sulphate and ammonium. Sulphate contributions were very significant during the coastal period, contributing

up to 32% of the total mass. Although chlorides contributed the least to the total mass, on average, during clear biomass burning events where sharp increases in CO and organics were observed, chlorides made up the largest component of inorganic aerosol[MM12]. The maximum chloride concentration during the campaign reached 53 μg m^{-3}. High soil and vegetation chloride contents have been observed in savannah and coastal environments (Lobert et al., 1999;Andreae et al., 1996). The strong elevations of chloride signals observed, particularly during burning events BBP1, BBP2 and BBP4 are likely a result of emission of these chloride ions. Outside of the "burning events" where very sharp increases in concentrations were observed, chloride concentrations were very low. This either suggests that these chloride species are short-lived, or only present in fires very close to the coast and therefore the ATARS site. [MM13]

Page 32: [41] Formatted **Marc Mallet** **11/8/16 11:22:00 PM**

Font:Not Bold, Font color: Text 1

Page 32: [41] Formatted **Marc Mallet** **11/8/16 11:22:00 PM**

Font:Not Bold, Font color: Text 1

Page 32: [41] Formatted **Marc Mallet** **11/8/16 11:22:00 PM**

Font:Not Bold, Font color: Text 1

Page 32: [41] Formatted **Marc Mallet** **11/8/16 11:22:00 PM**

Font:Not Bold, Font color: Text 1

Page 32: [41] Formatted **Marc Mallet** **11/8/16 11:22:00 PM**

Font:Not Bold, Font color: Text 1

Page 32: [42] Formatted **Marc Mallet** **11/8/16 11:22:00 PM**

Font:10 pt, Font color: Text 1

Page 32: [42] Formatted **Marc Mallet** **11/8/16 11:22:00 PM**

Font:10 pt, Font color: Text 1

Page 32: [42] Formatted Marc Mallet 11/8/16 11:22:00 PM

Font:10 pt, Font color: Text 1

Page 32: [42] Formatted Marc Mallet 11/8/16 11:22:00 PM

Font:10 pt, Font color: Text 1

Page 32: [42] Formatted Marc Mallet 11/8/16 11:22:00 PM

Font:10 pt, Font color: Text 1

Page 32: [42] Formatted Marc Mallet 11/8/16 11:22:00 PM

Font:10 pt, Font color: Text 1

Page 32: [42] Formatted Marc Mallet 11/8/16 11:22:00 PM

Font:10 pt, Font color: Text 1

Page 32: [42] Formatted Marc Mallet 11/8/16 11:22:00 PM

Font:10 pt, Font color: Text 1

Page 32: [42] Formatted Marc Mallet 11/8/16 11:22:00 PM

Font:10 pt, Font color: Text 1

Page 32: [42] Formatted Marc Mallet 11/8/16 11:22:00 PM

Font:10 pt, Font color: Text 1

Page 32: [42] Formatted Marc Mallet 11/8/16 11:22:00 PM

Font:10 pt, Font color: Text 1

Page 32: [42] Formatted Marc Mallet 11/8/16 11:22:00 PM

Font:10 pt, Font color: Text 1

Page 32: [42] Formatted Marc Mallet 11/8/16 11:22:00 PM

Font:10 pt, Font color: Text 1

Page 32: [42] Formatted Marc Mallet 11/8/16 11:22:00 PM

Font:10 pt, Font color: Text 1

Page 32: [42] Formatted **Marc Mallet** **11/8/16 11:22:00 PM**

Font:10 pt, Font color: Text 1

Page 32: [42] Formatted **Marc Mallet** **11/8/16 11:22:00 PM**

Font:10 pt, Font color: Text 1

Page 32: [42] Formatted **Marc Mallet** **11/8/16 11:22:00 PM**

Font:10 pt, Font color: Text 1

Page 32: [42] Formatted **Marc Mallet** **11/8/16 11:22:00 PM**

Font:10 pt, Font color: Text 1

Page 32: [42] Formatted **Marc Mallet** **11/8/16 11:22:00 PM**

Font:10 pt, Font color: Text 1

Page 32: [42] Formatted **Marc Mallet** **11/8/16 11:22:00 PM**

Font:10 pt, Font color: Text 1

Page 32: [42] Formatted **Marc Mallet** **11/8/16 11:22:00 PM**

Font:10 pt, Font color: Text 1

Page 32: [42] Formatted **Marc Mallet** **11/8/16 11:22:00 PM**

Font:10 pt, Font color: Text 1

Page 32: [42] Formatted **Marc Mallet** **11/8/16 11:22:00 PM**

Font:10 pt, Font color: Text 1

Page 32: [42] Formatted **Marc Mallet** **11/8/16 11:22:00 PM**

Font:10 pt, Font color: Text 1

Page 32: [42] Formatted **Marc Mallet** **11/8/16 11:22:00 PM**

Font:10 pt, Font color: Text 1

Page 32: [42] Formatted **Marc Mallet** **11/8/16 11:22:00 PM**

Font:10 pt, Font color: Text 1

Page 32: [42] Formatted **Marc Mallet** **11/8/16 11:22:00 PM**

Font:10 pt, Font color: Text 1

Page 32: [42] Formatted **Marc Mallet** **11/8/16 11:22:00 PM**

Font:10 pt, Font color: Text 1

Page 32: [42] Formatted **Marc Mallet** **11/8/16 11:22:00 PM**

Font:10 pt, Font color: Text 1

Page 32: [42] Formatted **Marc Mallet** **11/8/16 11:22:00 PM**

Font:10 pt, Font color: Text 1

Page 32: [42] Formatted **Marc Mallet** **11/8/16 11:22:00 PM**

Font:10 pt, Font color: Text 1

Page 32: [42] Formatted **Marc Mallet** **11/8/16 11:22:00 PM**

Font:10 pt, Font color: Text 1

Page 32: [42] Formatted **Marc Mallet** **11/8/16 11:22:00 PM**

Font:10 pt, Font color: Text 1

Page 32: [42] Formatted **Marc Mallet** **11/8/16 11:22:00 PM**

Font:10 pt, Font color: Text 1

Page 32: [42] Formatted **Marc Mallet** **11/8/16 11:22:00 PM**

Font:10 pt, Font color: Text 1

Page 32: [42] Formatted **Marc Mallet** **11/8/16 11:22:00 PM**

Font:10 pt, Font color: Text 1

Page 32: [42] Formatted **Marc Mallet** **11/8/16 11:22:00 PM**

Font:10 pt, Font color: Text 1

Page 32: [42] Formatted **Marc Mallet** **11/8/16 11:22:00 PM**

Font:10 pt, Font color: Text 1

Page 32: [42] Formatted	Marc Mallet	11/8/16 11:22:00 PM

Font:10 pt, Font color: Text 1

Page 32: [42] Formatted	Marc Mallet	11/8/16 11:22:00 PM

Font:10 pt, Font color: Text 1

Page 32: [42] Formatted	Marc Mallet	11/8/16 11:22:00 PM

Font:10 pt, Font color: Text 1

Page 32: [42] Formatted	Marc Mallet	11/8/16 11:22:00 PM

Font:10 pt, Font color: Text 1

Page 32: [42] Formatted	Marc Mallet	11/8/16 11:22:00 PM

Font:10 pt, Font color: Text 1

Page 32: [42] Formatted	Marc Mallet	11/8/16 11:22:00 PM

Font:10 pt, Font color: Text 1

Page 32: [42] Formatted	Marc Mallet	11/8/16 11:22:00 PM

Font:10 pt, Font color: Text 1

Page 32: [42] Formatted	Marc Mallet	11/8/16 11:22:00 PM

Font:10 pt, Font color: Text 1

Page 32: [42] Formatted	Marc Mallet	11/8/16 11:22:00 PM

Font:10 pt, Font color: Text 1

Page 32: [42] Formatted	Marc Mallet	11/8/16 11:22:00 PM

Font:10 pt, Font color: Text 1

Page 32: [42] Formatted	Marc Mallet	11/8/16 11:22:00 PM

Font:10 pt, Font color: Text 1

Page 32: [42] Formatted	Marc Mallet	11/8/16 11:22:00 PM

Font:10 pt, Font color: Text 1

Page 32: [42] Formatted **Marc Mallet** **11/8/16 11:22:00 PM**
Font:10 pt, Font color: Text 1

Page 32: [42] Formatted **Marc Mallet** **11/8/16 11:22:00 PM**
Font:10 pt, Font color: Text 1

Page 32: [42] Formatted **Marc Mallet** **11/8/16 11:22:00 PM**
Font:10 pt, Font color: Text 1

Page 32: [42] Formatted **Marc Mallet** **11/8/16 11:22:00 PM**
Font:10 pt, Font color: Text 1

Page 32: [42] Formatted **Marc Mallet** **11/8/16 11:22:00 PM**
Font:10 pt, Font color: Text 1

Page 32: [42] Formatted **Marc Mallet** **11/8/16 11:22:00 PM**
Font:10 pt, Font color: Text 1

Page 32: [42] Formatted **Marc Mallet** **11/8/16 11:22:00 PM**
Font:10 pt, Font color: Text 1

Page 32: [42] Formatted **Marc Mallet** **11/8/16 11:22:00 PM**
Font:10 pt, Font color: Text 1

Page 32: [42] Formatted **Marc Mallet** **11/8/16 11:22:00 PM**
Font:10 pt, Font color: Text 1

Page 32: [42] Formatted **Marc Mallet** **11/8/16 11:22:00 PM**
Font:10 pt, Font color: Text 1

Page 32: [42] Formatted **Marc Mallet** **11/8/16 11:22:00 PM**
Font:10 pt, Font color: Text 1

Page 32: [42] Formatted **Marc Mallet** **11/8/16 11:22:00 PM**
Font:10 pt, Font color: Text 1

Page 32: [42] Formatted **Marc Mallet** **11/8/16 11:22:00 PM**
Font:10 pt, Font color: Text 1

Page 32: [42] Formatted **Marc Mallet** **11/8/16 11:22:00 PM**
Font:10 pt, Font color: Text 1

Page 32: [42] Formatted **Marc Mallet** **11/8/16 11:22:00 PM**
Font:10 pt, Font color: Text 1

Page 32: [42] Formatted **Marc Mallet** **11/8/16 11:22:00 PM**
Font:10 pt, Font color: Text 1

Page 32: [42] Formatted **Marc Mallet** **11/8/16 11:22:00 PM**
Font:10 pt, Font color: Text 1

Page 32: [42] Formatted **Marc Mallet** **11/8/16 11:22:00 PM**
Font:10 pt, Font color: Text 1

Page 32: [42] Formatted **Marc Mallet** **11/8/16 11:22:00 PM**
Font:10 pt, Font color: Text 1

Page 32: [42] Formatted **Marc Mallet** **11/8/16 11:22:00 PM**
Font:10 pt, Font color: Text 1

Page 32: [42] Formatted **Marc Mallet** **11/8/16 11:22:00 PM**
Font:10 pt, Font color: Text 1

Page 32: [42] Formatted **Marc Mallet** **11/8/16 11:22:00 PM**
Font:10 pt, Font color: Text 1

Page 32: [42] Formatted **Marc Mallet** **11/8/16 11:22:00 PM**
Font:10 pt, Font color: Text 1

Page 32: [42] Formatted **Marc Mallet** **11/8/16 11:22:00 PM**
Font:10 pt, Font color: Text 1

Page 32: [42] Formatted	Marc Mallet	11/8/16 11:22:00 PM

Font:10 pt, Font color: Text 1

Page 32: [42] Formatted	Marc Mallet	11/8/16 11:22:00 PM

Font:10 pt, Font color: Text 1

Page 32: [42] Formatted	Marc Mallet	11/8/16 11:22:00 PM

Font:10 pt, Font color: Text 1

Page 32: [42] Formatted	Marc Mallet	11/8/16 11:22:00 PM

Font:10 pt, Font color: Text 1

Page 32: [42] Formatted	Marc Mallet	11/8/16 11:22:00 PM

Font:10 pt, Font color: Text 1

Page 32: [42] Formatted	Marc Mallet	11/8/16 11:22:00 PM

Font:10 pt, Font color: Text 1

Page 32: [42] Formatted	Marc Mallet	11/8/16 11:22:00 PM

Font:10 pt, Font color: Text 1

Page 32: [42] Formatted	Marc Mallet	11/8/16 11:22:00 PM

Font:10 pt, Font color: Text 1

Page 32: [42] Formatted	Marc Mallet	11/8/16 11:22:00 PM

Font:10 pt, Font color: Text 1

Page 32: [42] Formatted	Marc Mallet	11/8/16 11:22:00 PM

Font:10 pt, Font color: Text 1

Page 32: [42] Formatted	Marc Mallet	11/8/16 11:22:00 PM

Font:10 pt, Font color: Text 1

Page 32: [42] Formatted	Marc Mallet	11/8/16 11:22:00 PM

Font:10 pt, Font color: Text 1

Page 32: [42] Formatted **Marc Mallet** **11/8/16 11:22:00 PM**

Font:10 pt, Font color: Text 1

Page 32: [42] Formatted **Marc Mallet** **11/8/16 11:22:00 PM**

Font:10 pt, Font color: Text 1

Page 32: [42] Formatted **Marc Mallet** **11/8/16 11:22:00 PM**

Font:10 pt, Font color: Text 1

Page 32: [42] Formatted **Marc Mallet** **11/8/16 11:22:00 PM**

Font:10 pt, Font color: Text 1

Page 32: [43] Formatted **Marc Mallet** **11/8/16 11:22:00 PM**

Font color: Text 1

Page 32: [43] Formatted **Marc Mallet** **11/8/16 11:22:00 PM**

Font color: Text 1

Page 32: [43] Formatted **Marc Mallet** **11/8/16 11:22:00 PM**

Font color: Text 1

Page 32: [43] Formatted **Marc Mallet** **11/8/16 11:22:00 PM**

Font color: Text 1

Page 32: [43] Formatted **Marc Mallet** **11/8/16 11:22:00 PM**

Font color: Text 1

Page 32: [44] Formatted **Marc Mallet** **11/8/16 11:22:00 PM**

Font color: Text 1

Page 32: [44] Formatted **Marc Mallet** **11/8/16 11:22:00 PM**

Font color: Text 1

Page 32: [44] Formatted **Marc Mallet** **11/8/16 11:22:00 PM**

Font color: Text 1

Page 32: [44] Formatted	Marc Mallet	11/8/16 11:22:00 PM

Font color: Text 1

Page 32: [44] Formatted	Marc Mallet	11/8/16 11:22:00 PM

Font color: Text 1

Page 32: [44] Formatted	Marc Mallet	11/8/16 11:22:00 PM

Font color: Text 1

Page 32: [45] Moved to page 25 (Move #1)	Marc Mallet	5/2/17 1:32:00 AM

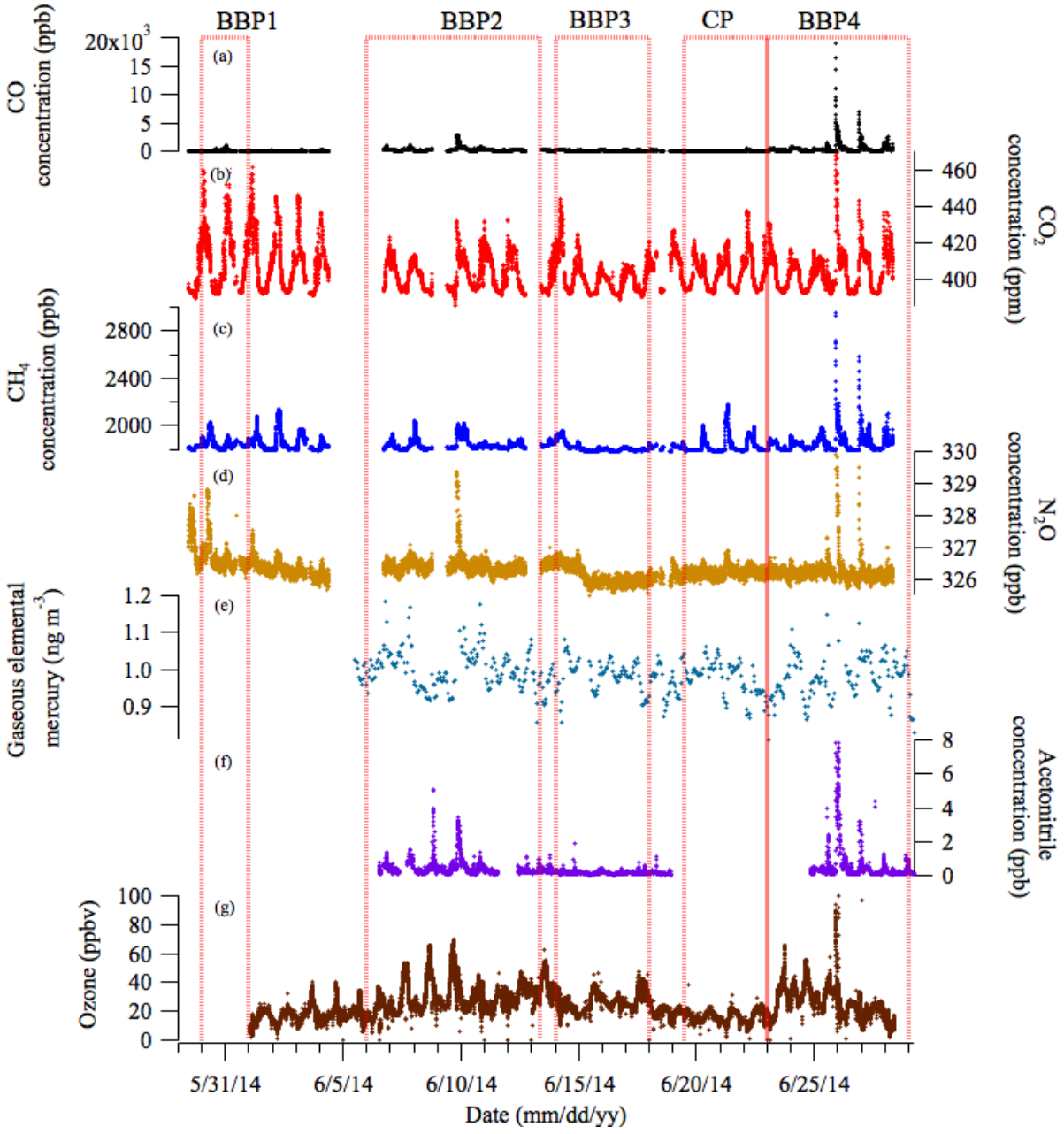

[MM14]

Figure **5** The time series of the major measured gaseous species during the SAFIRED campaign: (a) carbon monoxide, (b) carbon dioxide, (c) methane, (d) nitrogen dioxide[MM15], (e) gaseous elemental mercury, (f) acetonitrile and (g) ozone and $\Delta O_3/\Delta CO$. The biomass burning and coastal periods are indicated by the red dotted lines. All parts-per notation refer to mole fractions unless otherwise indicated.

Page 32: [46] Formatted	Marc Mallet	11/8/16 11:22:00 PM

Font color: Text 1

Page 32: [46] Formatted	Marc Mallet	11/8/16 11:22:00 PM

Font color: Text 1

Page 32: [46] Formatted	Marc Mallet	11/8/16 11:22:00 PM

Font color: Text 1

Page 32: [46] Formatted	Marc Mallet	11/8/16 11:22:00 PM

Font color: Text 1

Page 32: [46] Formatted	Marc Mallet	11/8/16 11:22:00 PM

Font color: Text 1

Page 32: [47] Moved to page 26 (Move #2)	Marc Mallet	5/2/17 1:32:00 AM

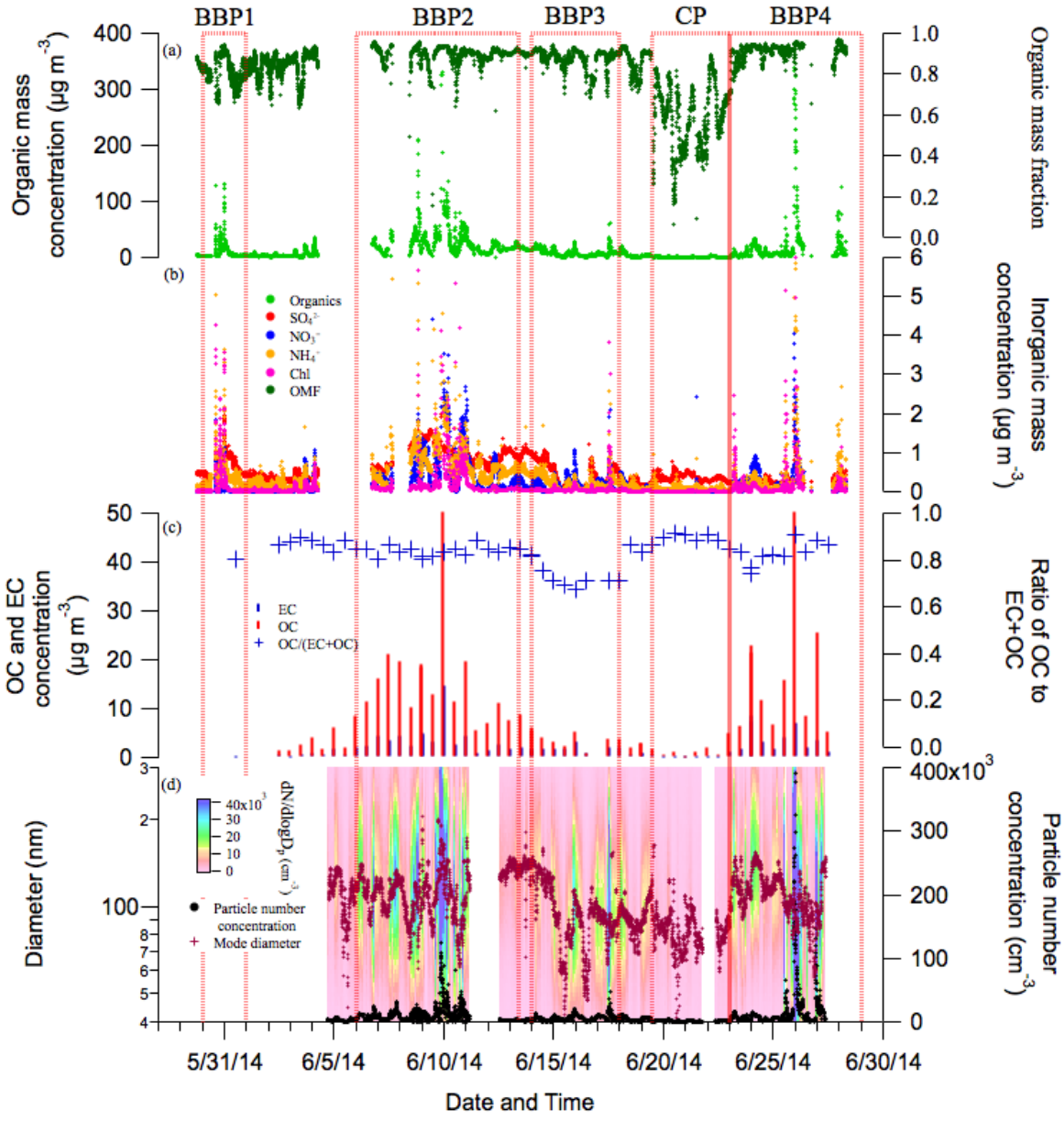

[MM16]

Figure **6** The times series of the major aerosol properties during the SAFIRED campaign: (a) the non-refractory PM_1 organic mass concentration (left) and organic mass fraction (right), b) the inorganic non-refractory PM_1 mass concentrations, (c) the 12-hour filter OC and EC PM_1 mass concentrations (left) and the ratio of OC to OC+EC (right), (d) the particle size distributions and particle size mode (left) and the total particle number concentration (right) and (e) the wind direction at ATARS.

Page 32: [48] Formatted	Marc Mallet	11/8/16 11:22:00 PM

Font color: Text 1

Page 32: [48] Formatted	Marc Mallet	11/8/16 11:22:00 PM

Font color: Text 1

Page 32: [48] Formatted Marc Mallet 11/8/16 11:22:00 PM

Font color: Text 1

Page 32: [48] Formatted Marc Mallet 11/8/16 11:22:00 PM

Font color: Text 1

Page 32: [48] Formatted Marc Mallet 11/8/16 11:22:00 PM

Font color: Text 1

Page 32: [48] Formatted Marc Mallet 11/8/16 11:22:00 PM

Font color: Text 1

Page 32: [48] Formatted Marc Mallet 11/8/16 11:22:00 PM

Font color: Text 1

Page 32: [48] Formatted Marc Mallet 11/8/16 11:22:00 PM

Font color: Text 1

Page 34: [49] Deleted Marc Mallet 5/14/17 10:42:00 PM

BBP1, BBP2 and BBP4 correspond to the periods when fires were burning within 10 km of ATARS. Large enhancements of biomass burning related emissions were observed during these three periods. There were distinct enhancements of all measured gaseous and aerosol species during these periods. Differences between the maximum and background concentrations were very prominent for CO (note the logarithmic scale in Figure 5a), CH_4, N_2O, acetonitrile (an established marker for biomass burning) and organic, nitrate and chloride non-refractory sub-micron aerosol species. Similar enhancements of CH_4 were also observed outside of these BB periods, which suggests another source of methane in this region. Only slight enhancements of GEM concentrations above background were observed during BBP2 and BBP4. Similar to much of the rest of the campaign sampling period, the non-refractory submicron aerosol was dominated by organics, with contributions typically varying between 70% and 95% of the mass. Relative to

background concentrations, there were also large enhancements of nitrate and chloride species during these periods. While there were also enhancements of sulfate and ammonium species during these periods, similar enhancements were observed outside of these periods, again indicating a non-fire source of these species. The ratio of O_3 to CO concentrations above background (taken as 10 ppbv and 66 ppbv, respectively) gives an indication of the photochemical age of a smoke plume. $\Delta O_3/\Delta CO$ were lowest during BBP2 and BBP4 (and not measured during BBP1) relative to the rest of the campaign, indicating that the biomass burning signals during these periods had not undergone extensive photochemical aging and are therefore characteristic of fresh smoke. [MM17]

Elevated signals during BBP1 were likely a result of a series of close fires within 5 km ENE of ATARS. The VIIRS and MODIS sensors on the SUMO NPP, Terra and Aqua satellites observes smaller fires at approximately 2 pm on the 30th of May. Winds were northeasterly during these two events. It is therefore likely that these signals were continuation or evolution of those fires. Burned vegetation was also visually observed the next morning at these locations. The large burst event later on the evening of the 31st of May is unlikely to be associated with these fires as the wind direction during this event was from the SSW and SSE. Large clusters of fires were observed at approximately 100 km and 150 km SE of the station by the Terra and Aqua satellites. The signals observed during this event could be a result of the plumes from this fire, although the possibility of a fire ignited after the satellite flyovers, or a combination of these cannot be eliminated.

Large signal enhancements on the 8th of June during BBP2 is likely a result of a cluster of fires approximately 100 km south east of the station. The MODIS sensors on the Terra and Aqua satellites observed the small cluster of fires along the back-trajectory at 11:14 am and 1:56 pm.

The source of BB emissions for the large event on the 9th of June during this period is unclear. Several fires approximately 5 km from the station along the back-trajectory were detected by the MODIS sensor on Aqua and the VIIRS sensor on SUOMI NPP at approximately 2:30 pm on the 9th of June. There were also numerous fires detected between 100 km and 200 km southeast along this trajectory. The signals associated with this event could therefore be a result of the closer fires that started to blaze later in the evening, the distant fires or a combination of both.

Only one fire within 20km of ATARS was observed during BBP3 on the 17th of June. Numerous fires were observed further than 20km from the station and is possible that the signals during this period were more aged. While photochemical aging and coagulation typically lead to larger particles, particle size distributions were smaller during this period and the ratio of OC to OC+EC was 70%, 10% lower than the ratio during the rest of the campaign. Whether these observations were a result of burn conditions or aging processes [MM18][MM19]

Page 34: [50] Deleted **Marc Mallet** **5/14/17 10:42:00 PM**

(i.e. evaporation of organic compounds from the aerosol phase) is unclear, although the highest $\Delta O_3/\Delta CO$ values during the campaign were observed during BBP3, which indicates photochemical aging was more extensive during this period.

One close fire was also observed during CP, however wind directions during this period were typically north-easterly and concentrations were therefore much lower. 5-day HYSPLIT trajectories also show that air mass during the CP originated along the east coast of Australia before travelling towards the sampling station with very little terrestrial influence.

Close proximity fires[MM20]

With numerous fires occurring across the region and the limitations of once-per-day satellite fly-overs and stationary measurements, it can be difficult to identify the exact source of these elevated signals. For a portion of BBP4, however, fires were burning within several kilometers of ATARS and several plumes were easily observed from the station. The signals from these plumes are shown in Figure 8. The observed enhancements between 12:30 pm and 3:00 pm on the 25th June during BBP4 were a result of grass fires burning approximately 1 km south-east from the station. During this event, the wind direction (Figure 8k) was highly variable, changing between 140° and 80° True Bearing (TB) multiple times. As a result, the sampling changed from measuring the air mass with and without the plume from this fire, which led to sharp increases and decreases in biomass burning-related signals (Figure 8a through 8j). Visually, the fire area and extent of the plume was larger at 4:00pm than earlier, however the wind direction changed to north-easterly which directed the plume away from the station. From 4:00 pm until 10:00 pm, the wind direction was stable at approximately 50° TB. At 10:00 pm, the wind direction rapidly changed to directly south and the largest enhancements for the whole campaign were observed until approximately 2:00 am on the 26th of June. It is very likely that these signals were a result of a continuation and evolution of these fires as the night progressed. Portions of a ~0.25 km^2 grassland field within 500 m directly south of ATARS were observed to be burned upon arrival at the station on the morning of the 26th of June and we speculate that the burning of this field contributed to the large enhancements in measured biomass burning emissions. The emissions during this portion of BBP4 are likely to be the most representative of fresh biomass burning smoke during the SAFIRED campaign. [MM21]

Page 34: [51] Moved to page 30 (Move #3) Marc Mallet 5/2/17 1:36:00 AM

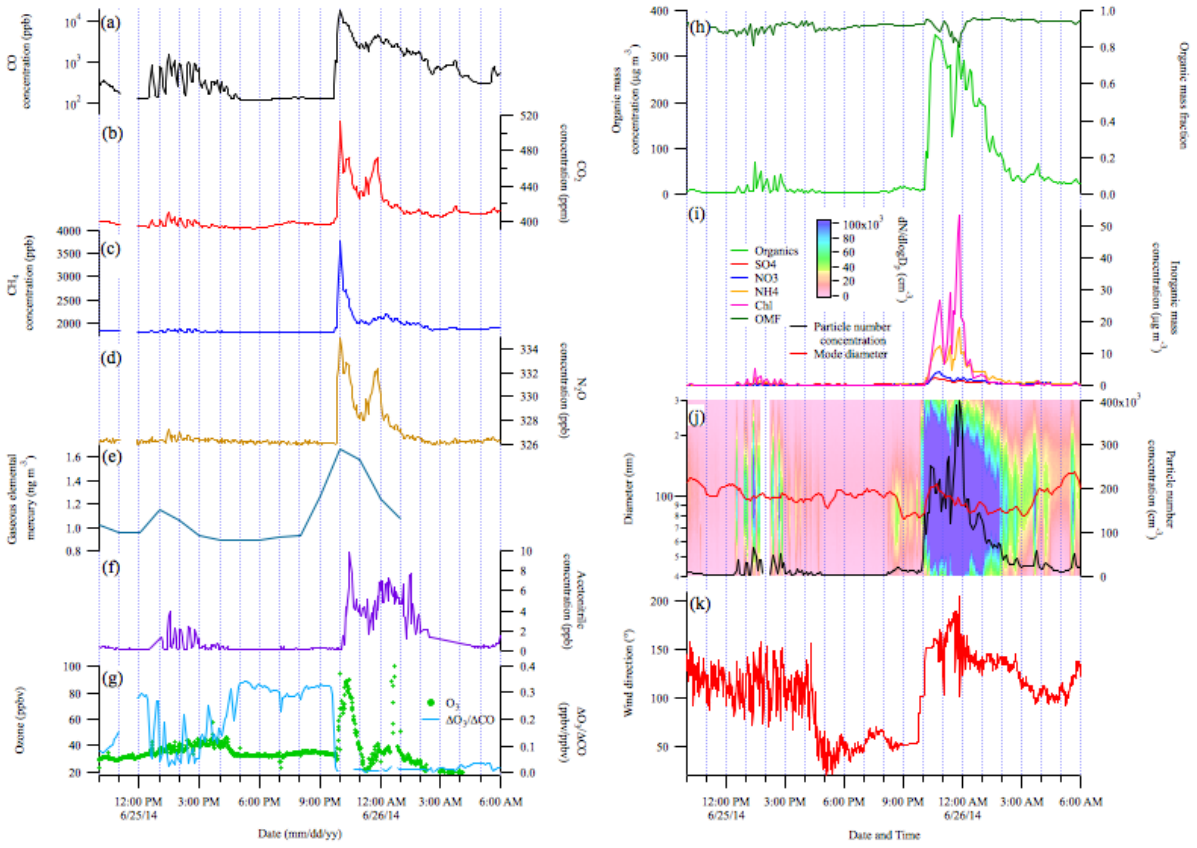

[MM22][MM23]

Figure 8 The major gas and aerosol concentrations measured during two biomass burning events within 1 km of ATARS during BBP4. (a) through (g) and (h) through (k) are as per Figures 5 and 6, respectively. All parts-per notation or mole fractions unless otherwise indicated.

Page 34: [52] Commented	Marc Mallet	3/20/17 4:36:00 PM

R3:

11. The 'Outcomes' section could benefit from the following: (i) discussion of the re- sults in the context of earlier work and how the findings here are similar or different, (ii) how the SAFIRED measurements were insightful (iii) what questions still remain unanswered, and (iv) directions for future work.

Page 34: [53] Commented	Marc Mallet	3/20/17 4:37:00 PM

R3:

12. Similar to comment 5, a Table listing the companion publications and its central finding would be helpful for the interested reader to track the measurement-specific paper.

Page 37: [54] Deleted	Marc Mallet	5/14/17 10:49:00 PM

Australian fires are responsible for 6% of global CO_2 biomass burning emissions, most of which is due to savannah fires (Shi et al., 2015). Carbon sequestering during regrowth periods is considered to balance carbon emissions in tropical Australia (Haverd et al., 2013). Greenhouse gases emitted from savannah fires that are not sequestered, such as methane (CH_4) and nitrous oxide (N_2O), have been shown to contribute 2-4% of the annual accountable greenhouse gas emissions from Australia (Meyer et al., 2012). Seasonal emission factors for the major greenhouse gases are important for national greenhouse gas inventories and in understanding the impact of savannah fires. Furthermore, emission factors of CO_2 and CO can be used to infer mechanisms behind the emissions of other species, such as the connection between particulate matter and burning conditions.

Page 37: [55] Formatted **Marc Mallet** **11/8/16 11:22:00 PM**

Font color: Text 1

Page 37: [56] Formatted **Marc Mallet** **11/8/16 11:22:00 PM**

Font color: Text 1

Page 37: [57] Formatted **Marc Mallet** **11/8/16 11:22:00 PM**

Font color: Text 1

Page 37: [58] Formatted **Marc Mallet** **11/8/16 11:22:00 PM**

Font color: Text 1

Page 37: [59] Formatted **Marc Mallet** **11/8/16 11:22:00 PM**

Font color: Text 1

Page 37: [60] Formatted **Marc Mallet** **11/8/16 11:22:00 PM**

Font color: Text 1

Page 37: [61] Formatted **Marc Mallet** **11/8/16 11:22:00 PM**

Font color: Text 1

The gaseous and aerosol data for the sample period were investigated to identify BB events and determine the emission factors of CO_2, CO, CH_4. N_2O, as well as Aitken and Accumulation mode aerosols and submicron particle species (organics, sulfates, nitrates, ammonium and chlorides) for several individual BB events. These emission factors were mostly found to be dependent on the combustion conditions (using the modified combustion efficiency as a proxy) of the fires. These results will be the first set of emission factors for aerosol particles from savannah fires in Australia. Furthermore, the variability in emission factors for different fires calls for a separation of single-value emission factors that are usually reported for savannah fires into grass and shrub components. A full discussion of these results are presented in Desservettaz et al. (2016, submitted).

Non-methane organic compounds (NMOCs)[MM24]

Biomass burning is the second largest source of NMOCs globally with a recent global estimate of at least 400 Tg $year^{-1}$, second only to biogenic sources (Akagi et al., 2011). Biomass burning produces a complex mix of NMOCs, which may be saturated or unsaturated, aliphatic or aromatic, and contain substitutions of oxygen, sulfur, nitrogen, halogens and other atoms. NMOC emission rates are strongly tied to the efficiency of combustion, with smouldering fires emitting NMOC at higher rates than flaming fires (Andreae and Merlet, 2001). Biomass burning derived NMOCs fuel the production of tropospheric ozone in diluted, aged biomass burning plumes, with higher ozone enhancements observed when biomass burning plumes interact with NOx-rich urban plumes (Jaffe and Wigder, 2012;Wigder et al., 2013;Akagi et al., 2013). Oxidation of NMOCs results in lower volatility products that partition to the aerosol phase and contribute significantly to secondary organic aerosol (Hallquist et al., 2009). Biomass burning produces significant amounts of semi-

volatile NMOC which can be difficult to quantify and identify with current measurement techniques. However recent studies have shown that including semi volatile NMOC chemistry in models improves the agreement between the modeled and observed organic aerosol (Alvarado et al., 2015; Konovalov et al., 2015) and ozone (Alvarado et al., 2015). High quality NMOC emission factors are crucial for models to assess the impact of biomass burning plumes on air quality and climate.

PAHs

Polycyclic aromatic hydrocarbons (PAHs) are a group of chemicals that are formed and emitted during combustion processes. Globally, major sources include residential/commercial biomass burning, open-field biomass burning and vehicular emissions (Shen et al., 2013). In Oceania in 2007, 31% of PAH emissions were estimated to be attributed to deforestation and wildfires (Shen et al., 2013). With control strategies targeting and reducing vehicular emission of PAHs over the last few decades, the relative contribution of other emission sources, such as savannah fires, has increased (Friedman et al., 2013;Kallenborn et al., 2012;Wang et al., 2016). Although most of these emissions are in the gas-phase (Jenkins et al., 1996;Atkins et al., 2010), the particle-phase PAHs, such as benzo[a]pyrene (BaP), may have high genotoxicity (IARC., 2015). However, field-based studies on emissions of PAHs from open-field biomass burning, including savannah fires remain limited in Australia (Freeman and Cattell, 1990).

Emission factors of PAHs from biomass burning related to savannah fires in northern Australia will be estimated form the data collected during this campaign. This estimation will be based on the (background subtracted) concentrations of PAHs and CO_2 (and CO) during the events where biomass burning contributes most to these concentrations measured at the sampling site. The

concentrations of 13 major PAHs (gaseous plus particle-associated phase) varied from ~ 1 to over 15 ng m^{-3} within different BB events. In the gas phase, 3- and 4-ring compounds typically contributed ~ 90% to the sum concentrations whereas the particle-associated PAHs were dominated by 5- and 6-ring compounds (> 80%). Measured PAH concentrations were significantly higher (paired *t*-test, $P < <0.05$) during BB events E, F and G. For these events, concentrations of BaP exceeded the monitoring investigation level for atmospheric BaP in Australia (National-Environment-Protection-Council-Service-Corporation, 2011), i.e. 0.30 ng m^{-3}, by 66% (BB event E) and 200% (BB events F and G). A full discussion of these results can be found in (Wang et al., 2016, under review).

Mercury

The atmosphere is the dominant transport pathway for mercury globally, with emissions to the atmosphere from both natural and anthropogenic origins (Driscoll et al., 2013). Whilst our understanding of the natural cycling of mercury has improved markedly over the past decades (Pirrone et al., 2010), large uncertainties still exist; specifically, global emission estimates to the atmosphere from biomass burning currently range between 300 and 600 Mg $year^{-1}$ (Driscoll et al., 2013). In the atmosphere, mercury exists as one of three operationally-defined species: gaseous elemental mercury (GEM), gaseous oxidised mercury (GOM) and particulate-bound mercury (PBM), each with differing abundances, solubility and depositional characteristics and with in-air conversion between all three species possible (Lin and Pehkonen, 1999). Mercury can be scavenged from the atmosphere through both wet and dry depositional processes, and the monsoonal climate of northern Australia results in varying significance of each of these processes through the year (Packham et al., 2009). Upon deposition, mercury may be stored in plant tissue via stomatal or cuticular uptake (Rea et al., 2002) or sequestered within soils (Gustin et al., 2008).

Release from both of these pools is achieved from burning events that may volatilise or thermally desorb mercury from biomass and soil, respectively (Melendez-Perez et al., 2014). Subsequently this mercury pool is redistributed through the atmospheric pathway to ecosystems that may methylate mercury, thereby enhancing its bioavailability to the local food chain.

SAFIRED represents the first measurements of atmospheric mercury undertaken in the tropical region of the Australian continent. The mean observed GEM concentration over the study period was 0.99 ± 0.09 ng m^{-3}, similar to the average over that month (0.96 ng m^{-3}) for 5 other Southern Hemisphere sites and slightly lower than the average (1.15 ng m^{-3}) for 5 tropical sites (Sprovieri et al., 2016). Mean GOM and PBM concentrations were 11 ± 5 pg m^{-3} and 6 ± 3 pg m^{-3} respectively, representing 0.6 – 3.4% of total observed atmospheric mercury.

Atmospheric mercury measurements were available only during the final four identified burn events. During these events, spikes in GEM concentrations were observed, though there were no significant increases in GOM or PBM. Emission ratios calculated during the campaign were two orders of magnitude higher than those reported by Andreae and Merlet (2001), though those were from scrub, rather than grass, BB events (Desservettaz et al., 2016). Future outcomes from the SAFIRED campaign will focus on the use of micrometeorological techniques and the passive tracer radon to quantify delivery of atmospheric mercury to tropical savannah ecosystems. ATARS also now serves as an additional site measuring continuous GEM as part of the Global Mercury Observation System (GMOS), one of only two tropical observing sites in the Eastern Hemisphere and the third such site located in Australia.

Aging of aerosols

Page 37: [63] Formatted	Marc Mallet	11/8/16 11:22:00 PM

Font color: Text 1

Page 37: [64] Formatted	Marc Mallet	11/8/16 11:22:00 PM

Font color: Text 1

Page 37: [65] Formatted	Marc Mallet	11/8/16 11:22:00 PM

Font color: Text 1

Page 37: [66] Formatted	Marc Mallet	11/8/16 11:22:00 PM

Font color: Text 1

Page 37: [67] Formatted	Marc Mallet	11/8/16 11:22:00 PM

Font color: Text 1

Page 37: [68] Formatted	Marc Mallet	11/8/16 11:22:00 PM

Font color: Text 1

Page 37: [69] Formatted	Marc Mallet	11/8/16 11:22:00 PM

Font color: Text 1

Page 37: [70] Formatted	Marc Mallet	11/8/16 11:22:00 PM

Font color: Text 1

Page 37: [71] Formatted	Marc Mallet	11/8/16 11:22:00 PM

Font color: Text 1

Page 37: [72] Formatted	Marc Mallet	11/8/16 11:22:00 PM

Font color: Text 1

Page 37: [73] Formatted	Marc Mallet	11/8/16 11:22:00 PM

Font color: Text 1

Page 37: [74] Formatted Marc Mallet 11/8/16 11:22:00 PM

Font color: Text 1

Page 37: [75] Formatted Marc Mallet 11/8/16 11:22:00 PM

Font color: Text 1

Page 37: [76] Formatted Marc Mallet 11/8/16 11:22:00 PM

Font color: Text 1

Page 37: [77] Formatted Marc Mallet 11/8/16 11:22:00 PM

Font color: Text 1

Page 37: [78] Formatted Marc Mallet 11/8/16 11:22:00 PM

Font color: Text 1

Page 37: [79] Formatted Marc Mallet 11/8/16 11:22:00 PM

Font color: Text 1

Page 37: [80] Formatted Marc Mallet 11/8/16 11:22:00 PM

Font color: Text 1

Page 37: [81] Formatted Marc Mallet 11/8/16 11:22:00 PM

Font color: Text 1

Page 37: [82] Formatted Marc Mallet 11/8/16 11:22:00 PM

Font color: Text 1

Page 37: [83] Formatted Marc Mallet 11/8/16 11:22:00 PM

Font color: Text 1

Page 37: [84] Formatted Marc Mallet 11/8/16 11:22:00 PM

Font color: Text 1

Page 37: [85] Formatted Marc Mallet 11/8/16 11:22:00 PM

Font color: Text 1

Page 37: [86] Formatted	Marc Mallet	11/8/16 11:22:00 PM

Font color: Text 1

Page 37: [87] Formatted	Marc Mallet	11/8/16 11:22:00 PM

Font color: Text 1

Page 37: [88] Formatted	Marc Mallet	11/8/16 11:22:00 PM

Font color: Text 1

Page 37: [89] Formatted	Marc Mallet	11/8/16 11:22:00 PM

Font color: Text 1

Page 37: [90] Formatted	Marc Mallet	11/8/16 11:22:00 PM

Font color: Text 1

Page 37: [91] Formatted	Marc Mallet	11/8/16 11:22:00 PM

Font color: Text 1

Page 37: [92] Formatted	Marc Mallet	11/8/16 11:22:00 PM

Font color: Text 1

Page 37: [93] Formatted	Marc Mallet	11/8/16 11:22:00 PM

Font color: Text 1

Page 37: [94] Formatted	Marc Mallet	11/8/16 11:22:00 PM

Font color: Text 1

Page 37: [95] Formatted	Marc Mallet	11/8/16 11:22:00 PM

Font color: Text 1

Page 37: [96] Formatted	Marc Mallet	11/8/16 11:22:00 PM

Font color: Text 1

Page 37: [97] Formatted	Marc Mallet	11/8/16 11:22:00 PM

Font color: Text 1

Page 37: [98] Formatted Marc Mallet 11/8/16 11:22:00 PM

Font color: Text 1

Page 37: [99] Formatted Marc Mallet 11/8/16 11:22:00 PM

Font color: Text 1

Page 37: [100] Formatted Marc Mallet 11/8/16 11:22:00 PM

Font color: Text 1

Page 37: [101] Formatted Marc Mallet 11/8/16 11:22:00 PM

Font color: Text 1

Page 37: [102] Formatted Marc Mallet 11/8/16 11:22:00 PM

Font color: Text 1

Page 39: [103] Deleted Marc Mallet 5/14/17 10:54:00 PM

Atmospheric chemistry and radiative forcing will depend on how gaseous and aerosol emissions from fires age as they move and interact with each other and existing species in the atmosphere. Biomass burning aerosols can be involved in condensation and coagulation (Radhi et al., 2012), undergo water uptake (Mochida and Kawamura, 2004) form cloud droplets (Novakov and Corrigan, 1996), and be exposed to photochemical aging processes, including those involving the gaseous components of fire emissions (Keywood et al., 2011;Keywood et al., 2015). With a reported lifetime of 3.8 ± 0.8 days (Edwards et al., 2006), biomass burning aerosols are able to travel intercontinental distances (Rosen et al., 2000) and are therefore present in the atmosphere long enough for substantial changes due to aging. Furthermore, tropical convection is likely to affect the aging of BB emissions in the region around ATARS, due to the immediate proximity to the warm waters in the Timor Sea (Allen et al., 2008). This introduces further uncertainty to the effect of BB emissions on radiation flux.

Primary organic aerosol directly emitted from biomass burning can interact with NMOCs to change composition and mass, resulting in secondary organic aerosol (Hallquist et al., 2009)[MM25]. Photochemical oxidation of NMOCs occurs during the daytime by either hydroxyl radicals or ozone. Ozone is also typically produced in the aging processes of tropical biomass burning plumes when NMOCs can oxidise to produce peroxy radicals that react with NO. Photochemical reactions also may lead to an overall increase in total aerosol mass through the condensation of NMOCs onto existing particles (Reid et al., 1998;Yokelson et al., 2009;Akagi et al., 2012;DeCarlo et al., 2008). Some studies have shown the opposite, i.e., photo-oxidation can also lead to the evaporation of some primary organic constituents, resulting in an overall mass reduction (Hennigan et al., 2011;Akagi et al., 2012). With thousands of organic compounds in the atmosphere, each with different volatilities and potential reaction mechanisms, our understanding of secondary organic aerosol production is limited (Goldstein and Galbally, 2007;Keywood et al., 2011). Furthermore, secondary organic aerosol can also form through aqueous phase reactions where water-soluble organics dissolve into water on existing particles (Lim et al., 2010).

Further analysis into the aerosol chemical composition will elucidate the aging of early dry season biomass burning emissions. Fractional analysis (e.g., f44 and f60, the fraction of m/z 44 and m/z 60 to all organic masses, indicated oxygenation and BB sources, respectively) and factor analysis using positive matrix factorisation (PMF) of cToF-AMS data has been investigated over the entire sampling period. Outside of the periods of significant influence from BB events, three PMF-resolved organic aerosol factors were identified. A BB organic aerosol factor was found to comprise 24% of the submicron non-refractory organic mass, with an oxygenated organic aerosol factor and a biogenic isoprene-related secondary organic aerosol factor comprising 47% and 29%,

respectively. These results indicate the significant influence of fresh and aged BB on aerosol composition in the early dry season. The emission of precursors from fires is likely responsible for some of the SOA formation. A full discussion of these results can be found in Milic et al. (2016). Future analysis will investigate the gas and particle-phase composition for individual BB events.

Water uptake of aerosols

The water uptake by aerosols is determined by their size and composition, as well as the atmospheric humidity (McFiggans et al., 2006). The hygroscopic properties of all of the different components of an aerosol particle contribute to its total hygroscopicity (Chen et al., 1973;Stokes and Robinson, 1966). The presence of different water-soluble and water-insoluble organics and inorganics will therefore strongly influence water uptake. Furthermore, chamber studies that have investigated emissions from biomass fuels, both separately and in combination, have shown that the hygroscopic response can vary significantly depending on fuel type (Carrico et al., 2010). Understanding the water uptake of atmospheric aerosols is further complicated when considering other aging processes as described previously. Nonetheless, it is important to characterise the water uptake, as this will, in turn, influence other atmospheric chemistry processes, radiation scattering and absorption as well as cloud processing.

Biomass burning aerosols can act as cloud condensation nuclei if they are large enough for water to easily condense onto their surface, or if the particles have a large affinity for water due to their composition (Novakov and Corrigan, 1996). Ultimately, this means that BB emissions can lead to a higher number of cloud droplets. This is important in reflecting solar radiation and cooling the earth's surface. Cloud albedo is more susceptible to changes when cloud condensation nuclei

concentrations are relatively low (Twomey, 1991), such as in marine environments like the Timor Sea off the coast of northern Australia.

The water uptake of aerosols has been further investigated to identify the possible influence of early dry season BB in this region on cloud formation. The concentrations of cloud condensation nuclei at a constant supersaturation of 0.5% were typically of the order of 2000 cm^{-3} and reached well over 10000 cm^{-3} during intense BB events. Variations in the ratio of aerosol particles activating cloud droplets showed a distinct diurnal trend, with an activation ratio of 40% ± 20% during the night and 60% ± 20% during the day. The particle size distribution and the hygroscopicity of the particles were found to significantly influence this activation ratio. A full discussion of these results can be found in Mallet et al. (2016, submitted). Future analysis will elucidate the contribution of different biomass burning aerosol components on the hygroscopicity.

Trace metal deposition

The deposition and dissolution of aerosols containing trace metals into the ocean may provide important micronutrients required for marine primary production. Conversely, the deposition of soluble iron can trigger toxic algal blooms, such as Trichodesmium, in nutrient-poor tropical and subtropical waters (LaRoche and Breitbarth, 2005). Trichodesmium blooms require large quantities of soluble iron, of which aerosols are a source (Boyd and Ellwood, 2010;Rubin et al., 2011). To date, most studies have assumed that mineral dust aerosols represent the primary source of soluble iron in the atmosphere (Baker and Croot, 2010); however fire emissions and oil combustion are other likely sources (Ito, 2011;Schroth et al., 2009;Sedwick et al., 2007). A few studies have shown that iron contained in biomass burning emissions is significantly more soluble

than mineral dust (Guieu et al., 2005;Luo et al., 2008;Schroth et al., 2009) but, to date, no data exists for Australian fires.

The aim of the trace metal aerosol component of SAFIRED is to quantify, for the first time, the fractional solubility of aerosol iron, and other trace metals, derived from Australian dry season BB. The fractional iron solubility is an important variable determining iron availability for biological uptake. On a global scale, the large variability in the observed fractional iron solubility results, in part, from a mixture of different aerosol sources. Estimates of fractional iron solubility from fire combustion (1 - 60 %) are thought to be greater than those originating from mineral dust (1 - 2%) (Chuang et al., 2005;Guieu et al., 2005;Sedwick et al., 2007), and may vary in relationship to biomass and fire characteristics as well as that of the underlying terrain (Paris et al., 2010;Ito, 2011). Iron associated with BB may provide information with respect to BB inputs of iron to the ocean (Giglio et al., 2013;e.g. Meyer et al., 2008). The ATARS provides an ideal location to further investigate BB derived fractional iron solubility at the source. The results from this study can be found in Winton et al. (2016) and show that soluble iron concentrations from BB sources are significantly higher than those observed in Southern Ocean baseline air masses from the Cape Grim Baseline Air Pollution Station, Tasmania, Australia (Winton et al., 2015). Aerosol iron at SAFIRED was a mixture of fresh BB, mineral dust, sea spray and industrial pollution sources. The fractional iron solubility (2 - 12%) was relatively high throughout the campaign and the variability was related to the mixing and enhancement of mineral dust iron solubility with BB species.